CHALMERS

Flow Analysis in wavy pipes using Large Eddy Simulation

Supervisor : Lars Davidson

Co-Supervisors : Fredrik Innings,Michael Olsson and Arlov Dragana

SANKAR MENON CP

Department of Applied Mechanics
Division of Fluid Dynamics
Chalmers University of Technology
Göteborg, Sweden
Master's Thesis 2014:82

MASTER'S THESIS 2014:82

Flow Analysis in wavy pipes using Large Eddy Simulation

SANKAR MENON CP

Department of Applied Mechanics
Division of Fluid Dynamics
CHALMERS UNIVERSITY OF TECHNOLOGY
Göteborg, Sweden, 2014

Flow Analysis in wavy pipes using Large Eddy Simulation
Master's Thesis in Fluid Dynamics

Master's Thesis 2014:82
ISSN: 1652-8557

Department of Applied Mechanics
Division of Fluid Dynamics
Chalmers University of Technology
SE-41296, Göteborg
Sweden
Tel. +46 (0)31-772 1000

Reproservice / Department of Applied Mechanics
Göteborg, Sweden 2014

Abstract

Several types of heat exchangers are used in various industries depending on their applications and limitations. One of the most common arrangements for flow paths within a heat exchanger are counter-flow and parallel flow, which are manufactured at Tetra Pak Food Processing Unit, Lund. These long narrow pipes are given corrugation at the wall for enhanced efficiency. It was important to study and understand the flow and thermal distribution inside these pipes. In the current work, computation fluid dynamics (CFD) is used to understand and quantify these characteristics.

Current work is based a Large Eddy Simulation of the flow where it is possible to resolve most of the eddies and less is modeled. In the current work, an in-house Chalmers solver, CALC-BFC is used for analysis. In the early stages of the thesis, it was important to validate the CALC solver and numerical methodologies. Thus the code is compared with the commercial software ANSYS Fluent and Star-CCM+. Later on, several refined meshes are simulated to realize how much is resolved and whether that is sufficient enough.

Later on, study is done on the different implementations for the current problem and its repercussions is analysed. Once the code is validated enough, an attempt is given to understand the flow phenomenon and heat enhancement due to the corrugation given on the pipe. Finally, the height of the corrugation is varied, keeping the outer radius constant and results are presented.

Keywords : LES, heat exchangers, corrugated and wavy pipe, CALC, heat enhancement.

Acknowledgments

First of all, I would like to thank my family for supporting and encouraging me at all times.

I would like to express my gratitude to my supervisor, Prof. Lars Davidson, who has helped me immensely on understanding the basic concepts for this thesis. Discussions I had with him always turned out be really fruitful and motivating. I thank him for giving me the opportunity to work in this highly interesting project.

I would like to thank supervisors from TetraPak, Fredrik Innings, Michael Olsson and Arlov Dragana, with whom I had meetings quite often. I will not able to achieve what I have achieved, without those meetings and discussions. I would also like to thank, Fredrik Carlsson from FS Dynamics, whom I worked with in the early stages of this thesis, inputs I had was always knowledgeable and inspiration.

I would like to thank Ansuman who always had time for me to have lengthy discussions on the in-house CALC code. Also, thank Manan for bringing interesting discussions into concepts of CFD. Last but not the least, I would like to thank my friends and colleagues, at Chalmers for creating a stimulating atmosphere.

Sankar Menon,
Göteborg June, 2014

Contents

Chapter 1

Introduction

The general function of a heat exchangers is to transfer heat from one fluid to another. The basic component of a heat exchangers can be viewed as a tube with one fluid running through it and another fluid flowing by on the outside. Heat exchangers are typically classified according to flow arrangement and type of construction. The simplest heat exchangers is one for which the hot and cold fluids move in the same or opposite directions in a concentric tube (or double-pipe) construction. In the parallel-flow arrangement, the hot and cold fluids enter at the same end, flow in the same direction, and leave at the same end. In the counter-flow arrangement, the fluids enter at opposite ends, flow in opposite directions, and leave at opposite ends. Alternatively, the fluids may be in cross flow (perpendicular to each other), or shell-and-tube heat exchangers.

In this thesis, work is confined to analyzing the inner-tube design of a concentric heat exchanger. The inner tube is made corrugated to enhance the turbulence and thus the heat transfer. The fundamental aspect of study on the corrugated pipes as heat exchangers is to analyse how effective they can transfer the heat. Thus the turbulence and the convection is studied closely in these pipes. The perturbations or corrugation are given in the pipes to enhance the heat transfer, but giving the pressure drop and friction as a penalty. Another important aspect of the current thesis is to understand and validate the implementation of CFD in the current problem. The corrugated pipe geometry and the problem framework was formulated by Tetra Pak.

1.1 Background

Lots of work has been done on studying the effect of the geometries and sensitivity of different parameters to achieve effective heat transfer. Vicente et. al. [1] has studied experimentally the effect of different Prandtl numbers on the heat transfer with the severity index ($\phi = h^2/pd$)[1] taken as the measure of roughness given to pipe. The paper goes on to suggest that heat transfer enhances with increase in Prandtl number. Also, at low Reynolds numbers ($Re < 10000$), the most advantageous tubes are those with the highest severity index ($\phi > 3{\cdot}10^{-3}$) while at high Reynolds numbers ($Re = 10000 - 40000$), the best choice is to employ tubes with intermediate roughness ($\phi = 1 - 2 \times 10e^{-3}$).

Large eddy simulations of similar geometries are tried out in the two papers by

[1] where h is the height of the corrugation, p is the pitch and d is the diameter of the pipe

Mirzaei et al. [2] and [3]. One paper explains the effect of corrugation while changing the Prandtl number and in the other paper the influence of wave amplitude is investigated. In the latter, the inner radius is kept constant while increasing the height of corrugation. There is also lot of research done at TetraPak internal Flow-group on the different geometries and different turbulent models.

1.2 Framework

In this thesis, the study on these pipes are confined to computational analysis. Different turbulence models can be used to understand the flow. Selection of these turbulence models depends on the priorities of the simulation. Here Large Eddy Simulation (LES) on the corrugated pipes is selected based on the accuracy required near the walls and also, because the Reynolds number is low.

The report is divided into sections, starting with explaination about the geometry and case set up in chapter 2. Chapter 3 gives the governing equations and methodologies that are used for solving and analyzing the problem at hand. Chapter 4 explains how that variables are non-dimentionalized in the CALC code and methods used in the post-processing stage to convert back to dimensional variables. The in-house Chalmers code (CALC-BFC) results are compared with the commercial codes ANSYS Fluent and STAR-CCM+ for a standard geometry in Chapter 5. In Chapter 6 different cases are tried to reduce the computational time of the simulations. Later, in chapter 7 the current mesh is validated with more refined meshes. Chapter 8 includes general study of the flow and turbulence enhancement in the pipe with explanation of the thermal enhancement. To better understand the flow and thermal distribution, different geometries are studied in Chapter 9. Finally, conclusive remarks on a overall basis are given.

Chapter 2

Problem description

2.1 Geometry

The main structure and corrugation profile of the geometry was taken from Tetra Pak after a series of studies conducted in their internal research department. The actual heat exchanger geometry is a bundle of narrow, long corrugated tubes inside another tube as seen in figure 2.1(a). These tubes are very long compared to its diameter as seen from figure 2.1(b).

The length of the pipe used for the computational simulation is small compared to the actual heat exchanger pipe used in the industry. This simplification can be done since the sinusoidally corrugated pipe geometry is periodic in the streamwise direction. Also, for constant property flow in a duct of streamwise periodic cross section, the velocity distribution becomes independent of the streamwise coordinates at sufficiently large distances from the inlet. However, that will not be the case with the temperature along the length. But, it can be said that the shape of the temperature distributions will be same. By employing this, computation of the flow analysis can be simplified to a small representative periodic geometry rather than solving for the entire length of the actual pipe. These periodicity simplification of the pipe and channel flow is explained more in Shah et al. [4] and Patankar et al. [5].

The three dimensional figure of the analyzed geometry is given in figure 2.2(a) and a cut section of the corrugation is illustrated in figure 2.2(b) to better understand the corrugation profile with the values given in table 2.1.

Parameter	value
Height of the corrugation, 2a	0.3 mm
Length of the pipe, L	10 mm
Outer radius of the pipe, R_o	7.2 mm

Table 2.1: Geometric parameters (see figure 2.2(b))

2.2 Prescribed general parameters

To validate the CALC-BFC code with the commercial codes (chapter 5) and study the change in the geometry profile of the corrugation(chapter 9), the problem framework was set with the prescribed parameters given in table 2.2 and illustrated in figure 2.2.

(a) Tube bundle (b) Whole heat exchanger

Figure 2.1: Tetra Spiraflo heat exchanger [6] [7]

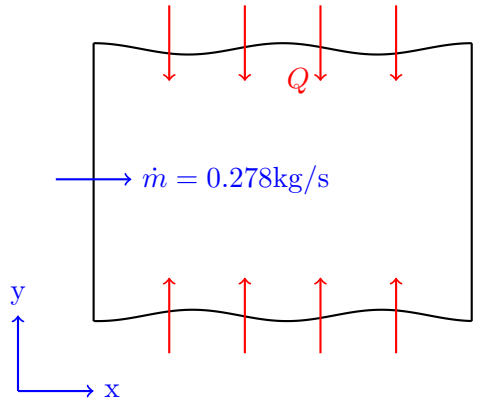

Figure 2.3: Illustration

Properties	Value
Density, ρ	996.95kg/m^3
Specific heat, C_p	4178J/kgK
Conductivity, k	0.606W/mK
Viscosity, μ	$9.03e^{-4}$kg/ms
Prandtl, Pr	6.23
Mass flow, $\dot{m}$	0.278kg/s
Reynolds number,Re_D	27220
Inlet T_b	$20°C$
Heat flux, Q	55 W

Table 2.2: Parameters for water at 25° C

These parameters for the problem statement was taken from TetraPak on the basis of their internal research.

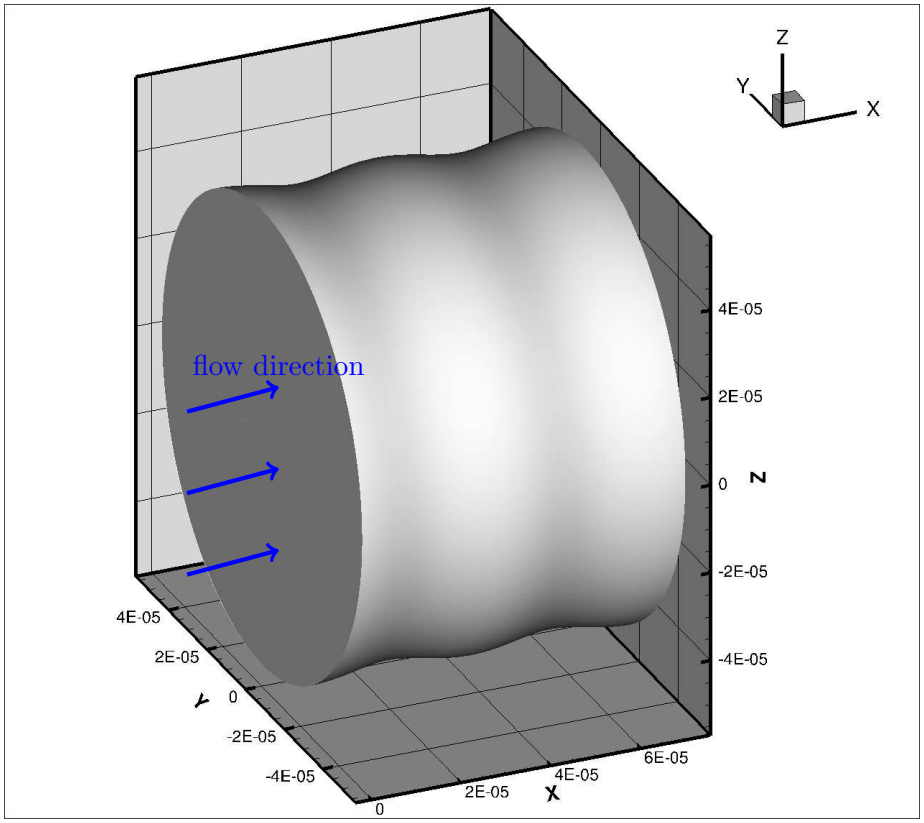

(a) 3D Geometry

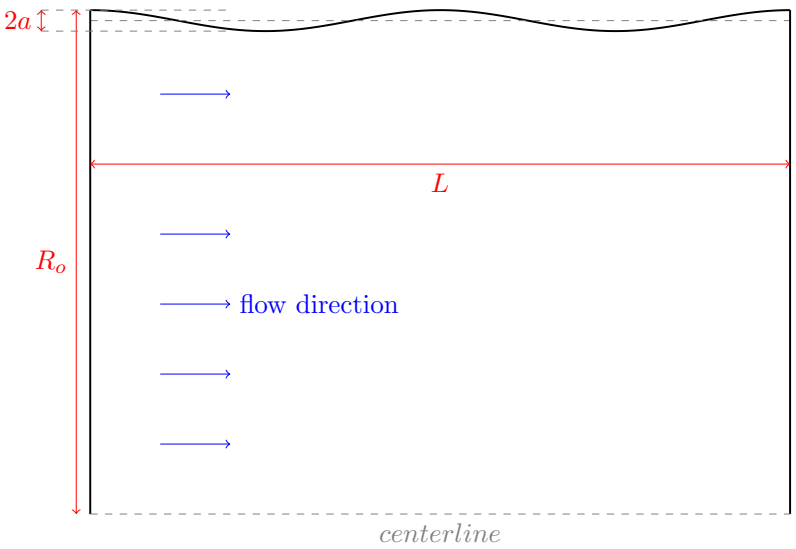

(b) 2D section of the pipe

Figure 2.2: Illustration of the corrugated pipe used for the analysis. L is the length, a is the amplitude of the corrugation and R_o is the outer radius.

Chapter 3

Governing equations and Numerical methodologies

The advancement of computational simulation of fluid flow has been tremendous over the past few decades. The advancements have happened both in the computational capabilities as well as the modeling techniques. Extensive software packages allow engineers to construct a geometry and boundary conditions to simulate a given viscous flow problem. The software then create a grid which splits the flow domain into finite volume cells and compute properties at each grid. These computations are not merely autonomous but rather require care and concern from the user. In particular if the flow Reynolds number goes from laminar to turbulent flow, the accuracy of the simulation is no longer assured in real sense. The reason is that turbulent flows are not completely resolved by the full equations of motion, and one resorts to using approximate turbulence models.

3.1 Navier-Stokes Equation

Simulations of physical systems necessarily involves simplifications by introduction of idealized abstractions in the form of models that aim at predicting the behavior of the systems. When modeling fluids, basic assumptions are made. Mass, momentum and energy are taken as conserved quantities and the continuum hypothesis is assumed to hold; it is assumed that molecular interactions in the fluid are of such large extent that fluctuations in the physical properties of the fluid evens out sufficiently to be described by continuous fields [8], [9]. From these assumptions, a set of equations modeling change in internal energy and motion of the fluid can be formulated [10]. Further assumptions about the nature of the fluid introduces the concept of in-compressible fluids as fluids where pressure variations have no significant effect on the density. As a result the continuity equation for incompressible fluids, describing mass conservation, takes a particularly simple form

$$\frac{\partial u_i}{\partial x_i} = 0, \tag{3.1}$$

where u_i is the velocity field and subscript i corresponding tensor notation according to Einstein's summation convention. Together with the assumption of constant viscosity, and neglecting all kinds of body forces (source terms), the momentum equations can be formulated as

$$\frac{\partial u_i}{\partial t} + \frac{\partial u_i u_j}{\partial x_j} = -\frac{1}{\rho}\frac{\partial p}{\partial x_j} + \nu \frac{\partial^2 u_i}{\partial x_j \partial x_j}, \tag{3.2}$$

where ν is the kinematic viscosity. This is called the *Navier-Stokes* equations.

The energy equation is then written as

$$\frac{\partial T}{\partial t} + \frac{\partial u_j T}{\partial x_j} = \frac{\nu}{Pr}\frac{\partial^2 T}{\partial x_j \partial x_j}, \tag{3.3}$$

where the Prandtl number is $Pr = (\nu \rho c_p)/k$, k is the thermal conductivity, ρ is density, c_p is specific heat.

3.2 Why Large Eddy Simulations (LES)?

Reynolds Averaged Navier Stokes (RANS) equation is obtained when the Navier Stokes equation is time averaged over a long period of time. The stress term that appears when the equation is time averaged is modeled. Thus all the turbulence is modeled, giving a "inaccuracy". But in the case of Large Eddy Simulation (LES), most of the eddies are resolved and only some of the smaller eddies are modeled. It was introduced after careful consideration that the most of the flow properties and information is carried in the large eddies. The small eddies are repetitive, similar, isotropic and do not depend on the geometry or the flow pattern around it, thus can be modeled. In LES, a spatial filtering operation that smoothens the turbulent behavior by removing the smallest spatial scales is introduced. When specially filtered, a subgrid scale (sgs) stress tensor is introduced (like the Reynolds stress when time averaged). This stress tensor describes the interaction between SGS (i.e, modeled) scales with the resolved larger scales. There are different models for modeling the same, some of them are mentioned later in section 3.5.

The filtered the system of equations (3.1), (3.2) and (3.3) has the form

$$\frac{\partial \bar{u}_i}{\partial x_i} = 0, \tag{3.4}$$

$$\frac{\partial \bar{u}_i}{\partial t} + \frac{\partial \bar{u}_i \bar{u}_j}{\partial x_j} = -\frac{1}{\rho}\frac{\partial \bar{p}}{\partial x_i} + \frac{\partial}{\partial x_j}\left[(\nu + \nu_t)\frac{\partial \bar{u}_i}{\partial x_j}\right], \tag{3.5}$$

$$\frac{\partial \bar{T}}{\partial t} + \frac{\partial \bar{u}_j \bar{T}}{\partial x_j} = \frac{\partial}{\partial x_j}\left[\left(\frac{\nu}{\mathrm{Pr}} + \frac{\nu_t}{\mathrm{Pr}_t}\right)\frac{\partial \bar{T}}{\partial x_j}\right], \tag{3.6}$$

Here the overbar represents spatially filtering and ν_t is the subgrid scale turbulent viscosity which is modeled. Eddy viscosity models are presented later in section 3.5

3.3 Numerical method for CALC

An incompressive finite volume code is used in the analysis. For space discretisation, a hybrid scheme of central differencing and van-leer is used for the all the velocity equations and pure van-leer is used for the temperature. The Crank-Nicolson scheme is used for time discretisation of all equations. The numerical procedure is based on an implicit, fractional step technique with a multigrid pressure Poisson solver (Emvin,[11]) and a non-staggered grid arrangement. The numerical procedure is explained in the Davidson and Peng [12].

3.4 Boundary Conditions

Setting up the boundary conditions that represent the actual physical conditions is a critical stage in CFD implementation. It needs to be noted that the computed geometry is half of the actual physical one. That is, only a half cylinder is simulated. The plane through symmetry axis of the cylinder has symmetric boundary condition and no-slip condition is assumed for the outer wavy wall. Also, a prescribed uniform constant heat flux is given at the outer wall as per the required problem.

An important boundary condition for current cylinder flow is the periodic boundary condition. A source term appears in energy and momentum equations to implement this boundary condition. Periodic conditions for a cylinder flow are well explained in the paper by Patankar et al. [5]. A brief note on the same is written here.

The Navier-Stokes equation for the periodic cylinder flow for an incompressible viscous flow is,

$$\frac{\partial \bar{u}_i}{\partial t} + \frac{\partial \bar{u}_i \bar{u}_j}{\partial x_j} = \beta \delta_{1i} - \frac{1}{\rho}\frac{\partial \bar{p}}{\partial x_i} + \frac{\partial}{\partial x_j}\left[(\nu + \nu_t)\frac{\partial \bar{u}_i}{\partial x_j}\right], \tag{3.7}$$

$$\frac{\partial \bar{T}}{\partial t} + \frac{\partial \bar{u}_j \bar{T}}{\partial x_j} = \frac{\partial}{\partial x_j}\left[\left(\frac{\nu}{\mathrm{Pr}} + \frac{\nu_t}{\mathrm{Pr}_t}\right)\frac{\partial \bar{T}}{\partial x_j}\right] - \gamma \bar{u}_1. \tag{3.8}$$

It is same as equations 3.5 and 3.6, except that a source term appears in each equation. The pressure field is subdivided into two terms as,

$$p(x,y,z) = -\beta x + P(x,y,z). \tag{3.9}$$

The βx term, which comes due to periodicity, is related to the global mass flow and $P(x,y.z)$ is related to the detailed local motions. The quantity β can be regarded as an assignable parameter, the given values of which will generate corresponding mass flows (Reynolds number). The β value can also be set to time varying, while keeping the mass flow with a prescribed value. The details of this implementation is given in the Section 6.1.

Other boundary conditions would be,

$$Solid: \quad u = v = 0 \tag{3.10}$$

$$Symmetry: \quad \partial u/\partial y = 0, \qquad v = 0 \tag{3.11}$$

$$\phi(x,y,z) = \phi(x+L,y,z), \qquad \phi = u,v,P \tag{3.12}$$

For the constant heat flux, the temperature periodic condition is given as,

$$T(x,y,z) = \gamma x + \hat{T}(x,y,z) \tag{3.13}$$

Furthermore, $\hat{T}$ is periodic. Also, it can be shown that $\gamma = \dot{q}/\dot{m}c_p$, where $\dot{q} = Q/A_{wall}$, Q is the heat flux.

3.5 Subgrid-scale modeling

In the LES approach, turbulent scales smaller than the grid size are not resolved. They are considered through the subgrid scale tensor T_{ij} given by

$$T_{i,j} = \overline{u_i u_j} - \overline{u_i}\,\overline{u_j} \tag{3.14}$$

where overbar represents the filtration of variables below which it is modeled.

The simplest model is the Smagorinsky's model in which the eddy-viscosity is assumed to be proportional to the subgrid characteristic length scale $\Delta = (\Delta x \Delta y \Delta z)^{1/3}$ and to a characteristic turbulent velocity taken as the local strain rate $|\overline{S}|$,

$$\nu_t = (C_s\Delta)^2|\overline{S}|, \text{ where} |\overline{S}| = \sqrt{2\overline{S_{ij}}\overline{S_{ij}}}. \tag{3.15}$$

Near the wall, the SGS viscosity becomes quite large since the velocity gradient is very large. However, since the SGS turbulent fluctuations at the walls go to zero, so must the SGS viscosity. A damping function f_μ is added to ensure this, [13]

$$f_\mu = 1 - \exp(-x_2^+/26) \tag{3.16}$$

This model is further developed in the dynamic Smagorinsky model (DSM) of Germano et al. [14] and with modification by Lilly [15]. The near-wall behavior of the DSM model in wall-resolving LES is such that it yields an eddy viscosity which is reduced naturally by the dynamic procedure as the wall is approached. Hence no explicit damping is required.

As mentioned using DNS by Wray and Hunt [16], energy is concentrated in the streams and energy dissipation in the eddies and convergence zones. The classical Smagorinsky does not account for the former which are regions where the vorticity dominates the irrotational strain. On the other hand, the dominant deformation in the convergence zones is the irrotational strain so that strain rate is good measure of the dissipative activity. Thus a better model based on both $|\bar{S}|$ and rotational rate was introduced by Ducros and Nicoud [17] [18] known as the wall-adaptive local eddy-viscosity (WALE) model. This model is used for the major part of study in this thesis.

Viscosity using the WALE model is given as,

$$\nu_{sgs} = (c_w\Delta)^2 \frac{(s_{ij}^d s_{ij}^d)^{3/2}}{(\bar{s_{ij}}\bar{s_{ij}}^{5/2} + s_{ij}^d s_{ij}^d)^{5/4}}, \tag{3.17}$$

$$s_{ij}^d = \frac{1}{2}(\overline{g}_{ij}^2 + \overline{g}_{ji}^2) - \frac{1}{3}\delta_{ij}\overline{g}_{kk}^2, \;\; \overline{s}_{ij} = \frac{1}{2}\left(\frac{\partial \overline{u}_i}{\partial x_j} + \frac{\partial \overline{u}_j}{\partial x_i}\right)$$

Chapter 4

Non-dimentionalizing variables

When comparing different data, it is always convenient to have variables in a generalized dimensionless form. However in this report, since the variables handled in commercial codes are in their dimensional form, variables from CALC solver are converted back to dimensional form. Before moving into the CALC validation with commercial codes (chapter 5) and general flow analysis, a general clarity and understanding of these variable was considered beneficial.

A brief description of the variables in the non-dimensional form in the in-house CALC solver are shown below.

- The inlet mass flow is set such that inlet bulk velocity, u_b, is unity.
- All geometrical parameters are non-dimentionalized by a divisional factor of outer radius of the corrugated pipe.
- The momentum equation is divided by density and the energy equation is divided by density and specific heat, C_p.
- Prescribed heat flux which comes as source term in energy equation is given the value 10^{-3}. (see (4.6))

The physical properties of the fluid are described with two parameters, viscosity and Prandtl number.

4.0.1 Reynolds Number

Reynolds number is a dimensionless variable, which includes flow speed (velocity), geometry (characteristic length) and fluid property (viscosity). It is the primary parameter that correlates the viscous behavior of all Newtonian fluids. Reynolds number can be defined using different parameters. One way is to define in terms of radius at the inlet of the pipe (i,e *characteristic length* will be the inlet radius).

The Reynolds number is defined as,

$$Re_R = \frac{u_b r}{\nu}, \tag{4.1}$$

where u_b m/s is the bulk velocity at the inlet of the pipe, ν m^2/s is the dynamic viscosity and r is the radius at the inlet.

Reynolds number can also be defined in terms of mass flow ($\dot{m}$ kg/m^3) as,

$$Re_R = \frac{\dot{m}}{\mu \pi r}. \tag{4.2}$$

Calculation for the current work : Here calculations to make the variables dimensionless are explained. For the commercial codes the mass flow is specified directly as $\dot{m} = 0.278\,\text{kg/sec}$. Here the characteristic length is chosen as the inlet radius of the pipe i.e, 7.2mm. Thus, Reynolds number according to equation 4.2, will be 13610.

In CALC code bulk velocity u_b, density and inlet radius is implemented with unit value. Thus, mass flow will be like: $\dot{m} = \rho u_b A_{inlet} = \pi\,\text{kg/s}$. The viscosity is implemented in the solver as $\nu = 1/13610$.

4.0.2 Heat transfer coefficient, h (W/m^2K)

Heat transfer coefficient (HTC), can be derived from Newtons's law of cooling in which the local heat convective flux is given as,

$$\dot{q} = h(T_s - T_\infty) \tag{4.3}$$

where h is the heat transfer coefficient, T_s and T_∞ are the surface and reference temperature respectively.

The equation HTC can be written as,

$$h = \frac{\dot{q}}{T_w - T_{bulk}} \tag{4.4}$$

where T_w is the wall temperature, T_{bulk} is the bulk temperature and $\dot{q}$ is the heat flux per unit area.

4.0.3 Temperature

The advective heat flux can be expressed as,

$$\dot{q} = \dot{m} c_P \Delta T \tag{4.5}$$

where, $\dot{q}$ is the heat flux per spanwise area (Q/A_{wall}), c_p is the specific heat capacity, $\dot{m}$ is the mass flow. Now, the source term in the energy equation (3.8) for this heat flux, in a periodic channel, is given as,

$$\gamma = \dot{q}/\dot{m} c_p, \tag{4.6}$$

The Calculations The temperature computed from the CALC solver is converted to its dimentional form in the post-processing stage. A step by step calculation of this process is explained here [1].

- Heat flux at the wall, as implemented in commercial codes, Q = 55W (54.2592W).
- The heat transfer per unit area,
  $\dot{q} = Q/A_{wall} = 60{,}000 W/m^2$,
  where $A_{wall} = 0.00090432 m^2$
- Now you calculate,
  $\sigma_D = \dot{q}/\rho c_P u_b = 0.0084K$,
  where, density $\rho = 996.95\text{kg/m}^3$, specific heat capacity $c_P = 4178\text{J/kgK}$ and bulk velocity $u_b = 1.712\text{m/s}$.

[1] Note : subscript D represents dimensional parameters and ND represents non-dimensional parameters.

- In CALC code sigma term is taken as $\sigma_{ND} = 10^{-3}K$. We have temperature in the domain, T_{ND} and $T_{bulk_{ND}}$ from the CALC solver. $T_{bulk_D} = 20$C.
- $\sigma/\Delta T$ is a non-dimensional term which can equated between the CALC code and the commercial codes as,

$$\frac{\sigma_D}{T_D - T_{bulk_D}} = \frac{\sigma_{ND}}{T_{ND} - T_{bulk_{ND}}}. \tag{4.7}$$

- Thus the temperature in dimensional form is computed as,

$$T_D = \frac{\sigma_D}{\sigma_{ND}}(T_{ND} - T_{bulk_{ND}}) + T_{bulk_D}. \tag{4.8}$$

4.0.4 Other variables

Other variables are non-dimentionalized by dividing by factors given in table 4.1.

Variable	Non-Dimentionalizing factor	Unit
Velocity, u	u_b	m/sec
Pressure, P	ρu_b^2	Pa
Wall shear stress, τ_w	ρu_b^2	Pa
Differential Pressure, P	$(\rho u_b^2)/(R)$	Pa/m

Table 4.1: Here u_b is the bulk velocity; R is the radius of the pipe.

Chapter 5

Validation of CALC-BFC with ANSYS Fluent and STAR CCM+

Major work of this thesis was devoted to validation of the CALC-BFC solver with the commercial solvers, Fluent and Star-CCM+. For validation, all the parameters and the geometries are identical for all three solvers. Fluent and Star-CCM+ uses common mesh and separate in-house mesh using G3D/MATLAB and FORTRAN code is created for CALC-BFC. These values were studied along the radial direction at the six different stream-wise equidistant locations as given in figure 5.1. These locations were selected so that it covers the entire periodic length and captures the re-circulation zone.

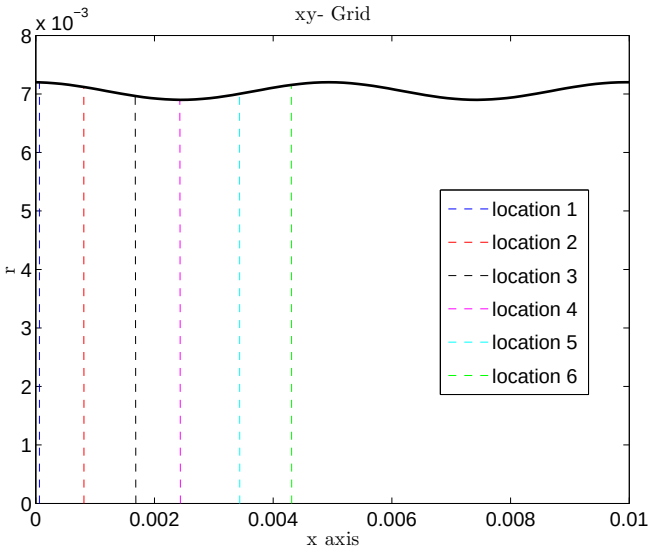

Location	x (m)
1	0
2	0.833
3	1.667
4	2.5
5	3.333
6	4.167

Figure 5.1: Figure shows the cut section of the wave pipe, where variables are studied along the radial direction (r) at six different x-locations

5.1 Setting for the comparison

While comparing three different solvers, the modeling/numerical schemes, mesh values and other modeling constants were kept to be identical. For the CALC solver, QUICK was first used for spacial scheme and later on changed to Hybrid Central- Van-Leer for velocity equation and pure Van Leer for temperature. The implemented values and schemes are shown in table 5.1.

	CALC-BFC	Fluent	Star-CCM+
Mesh	$82 \times 82 \times 258$ nodes	16.2 million cells	16.2 million cells
x^+	8.52	8.30	8.15
y^+	0.24	0.30	0.29
z^+	12.04	11	10.80
Length, L(mm)	10	20	20
Scheme	Implicit frac. step	SIMPLE	SIMPLE
Pressure	Multigrid Poisson solver	2nd Order	2nd Order
Energy eqn.	Van-Leer	2nd Order	QUICK
Momentum	Hybrid Central and Van-Leer	Central	Central
Time	Crank-Nicolson	Crank-Nicolson	Crank-Nicolson
WALE const (C_m)	0.325	0.544	0.325
Iter/time step	2	6	6

Table 5.1: Setting for the comparison. x^+, y^+ and z^+ values are taken at the inlet wall

The commercial solvers uses pipe geometry with four corrugations compared to two in CALC solver. Also, CALC uses half (180 degree) cylinder compared to full (360 degree) for commercial ones. Also, the commercial codes can run parallel, while CALC code has a limitation of running only on a single core processor. The start of sampling here is decided when the fluctuations of pressure and heat transfer coefficient are within the required limit, say 10% from the mean value.

5.2 Variable comparison

Velocity and temperature are compared from the momentum and energy Navier-Stokes equation, respectively.

5.2.1 Velocity

Streamwise velocity is compared among the solvers, at the locations given in figure 5.1. The velocities near the walls will be more sensitive to different solvers, thus, a logarithmic plot of velocity is also analyzed.

Near wall region

Figure 5.2 shows logarithmic velocities near the walls for three solvers. At locations 1 and 6, where there is minimal circulation, the velocity profile at the viscous region is similar to a plane channel flow. In other locations, this profile is being destroyed because of the circulation created by the corrugated wall. The velocities in the viscous region are accelerated as the flow enters the re-circulation regions.

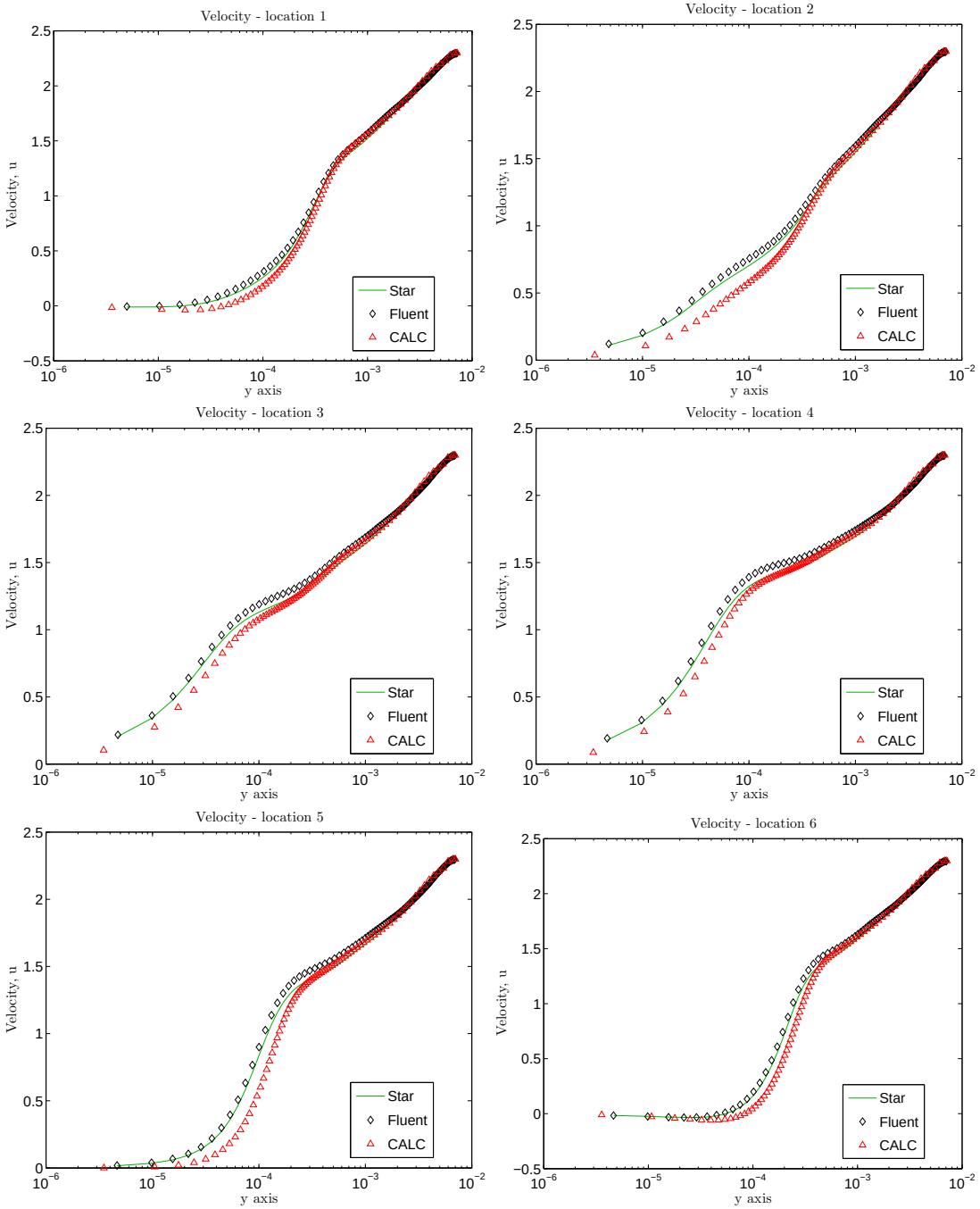

Figure 5.2: Comparative near wall logarithmic plots of the stream wise velocity $u\,or(v_1)\,\mathrm{m}^2/\mathrm{s}$ along the wall normal direction of all solvers.

The convergence of the momentum equation is quite sensitive to the velocities near the walls, thus comparison of the velocity profiles near the walls is a good benchmark. It can be seen from figure 5.2 that the velocities from the CALC solver matches well with the commercial solvers.

Along wall normal direction

In the addition to the near wall velocities in the Section 5.2.1, stream-wise velocities are shown in figure 5.3. These figures gives a better illustration of the velocity at the center of the pipe. Small deviation in the velocity near the walls reflected back at the center of the pipe, due to conservation of mass flow. For example, if the velocities was under predicted at the walls, it over predicts at the center and vise verse. This seems quite obvious but through the thesis it was realized that over prediction was more easily noticed than near wall under-prediction. This was evident through the study in section 6.2.

Circulation regions comparison

The re-circulation that the occurs at the flow separation regions of the wavy wall is also shown comparatively for Fluent in figure 5.4(b) and CALC-BFC in figure 5.4(a). Flooded contour in figure is given for negative stream-wise velocity (u). All positive u is given white color. The separation and the reattachment points are also seems to matching each other. A detailed explanation of the streamlines and vortices is explained in section 8.1

5.3 Temperature

After realizing that velocity matches quite well, temperature (energy) equation is analyzed in this section. Here temperature is compared for different solvers similar to the velocity in the previous section.

5.3.1 Near wall region

The temperature profile are compared at the same six location as shown in figure 5.1. Logarithmic plots of temperature near the walls are shown in figure 5.5. The values were satisfactory similar to proceed with the CALC solver.

5.3.2 Wall temperature

Since the temperature at the wall is really sensitive for the study of heat exchangers, they were compared for the three solvers as shown in figure 5.6.

5.4 HTC, h and Wall Shear Stress, τ_w

Furthermore, the heat transfer coefficient (h) and wall shear stress (W/m^2K) are compared between the solvers as shown on figures 5.7(a) and 5.7(b). The wall shear stress is the arguable a good parameter to compare the codes since it is computed near the wall and it is supposed to be most sensitive to turbulent fluctuations.

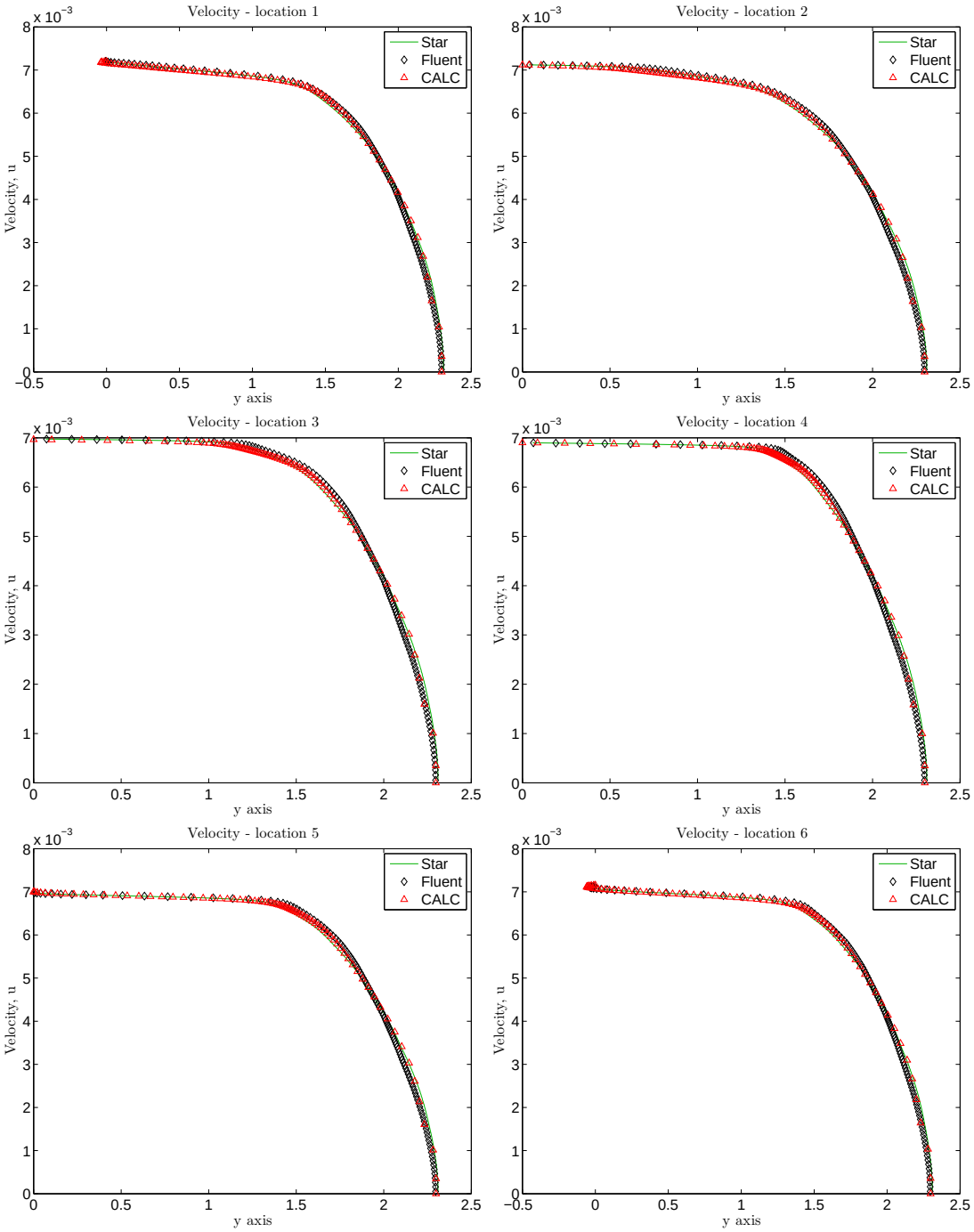

Figure 5.3: Stream-wise velocity $u, (v_1)\,\mathrm{m}^2/\mathrm{s}$ at six different locations along the wall normal directions are compared for all three solvers.

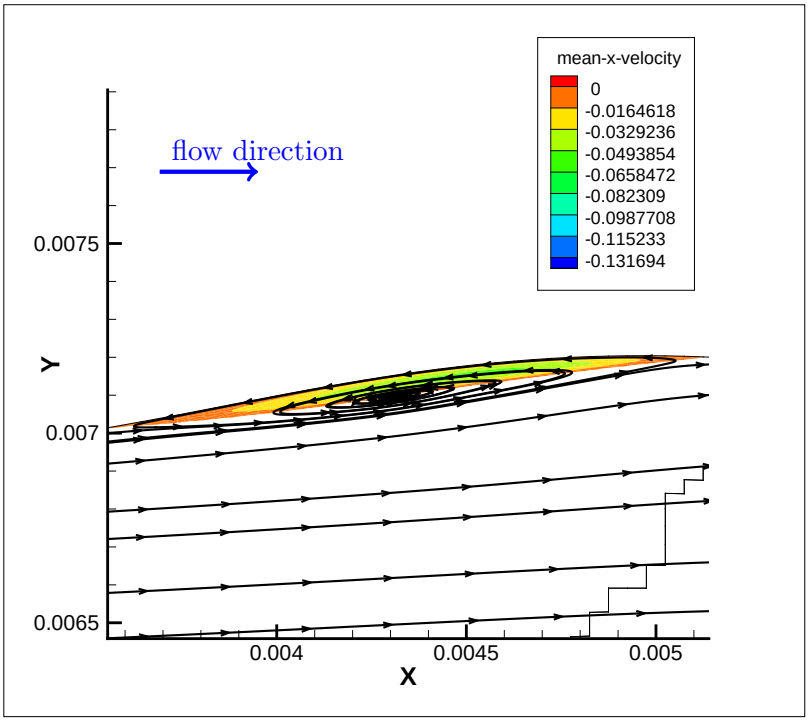

(a) Circulation in Fluent solver

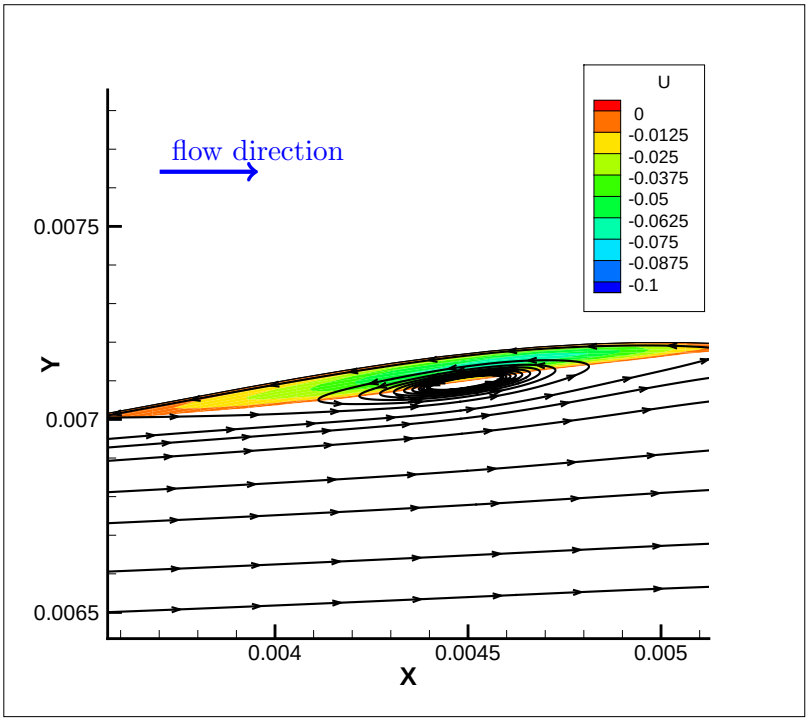

(b) Circulation in CALC-BFC solver

Figure 5.4: Circulation at the corrugated region of the pipe. Flooded contour is negative stream-wise velocity and positive velocity is given as blank white color. The integrated velocity streamlines is given with black solid lines, with their directions on them.

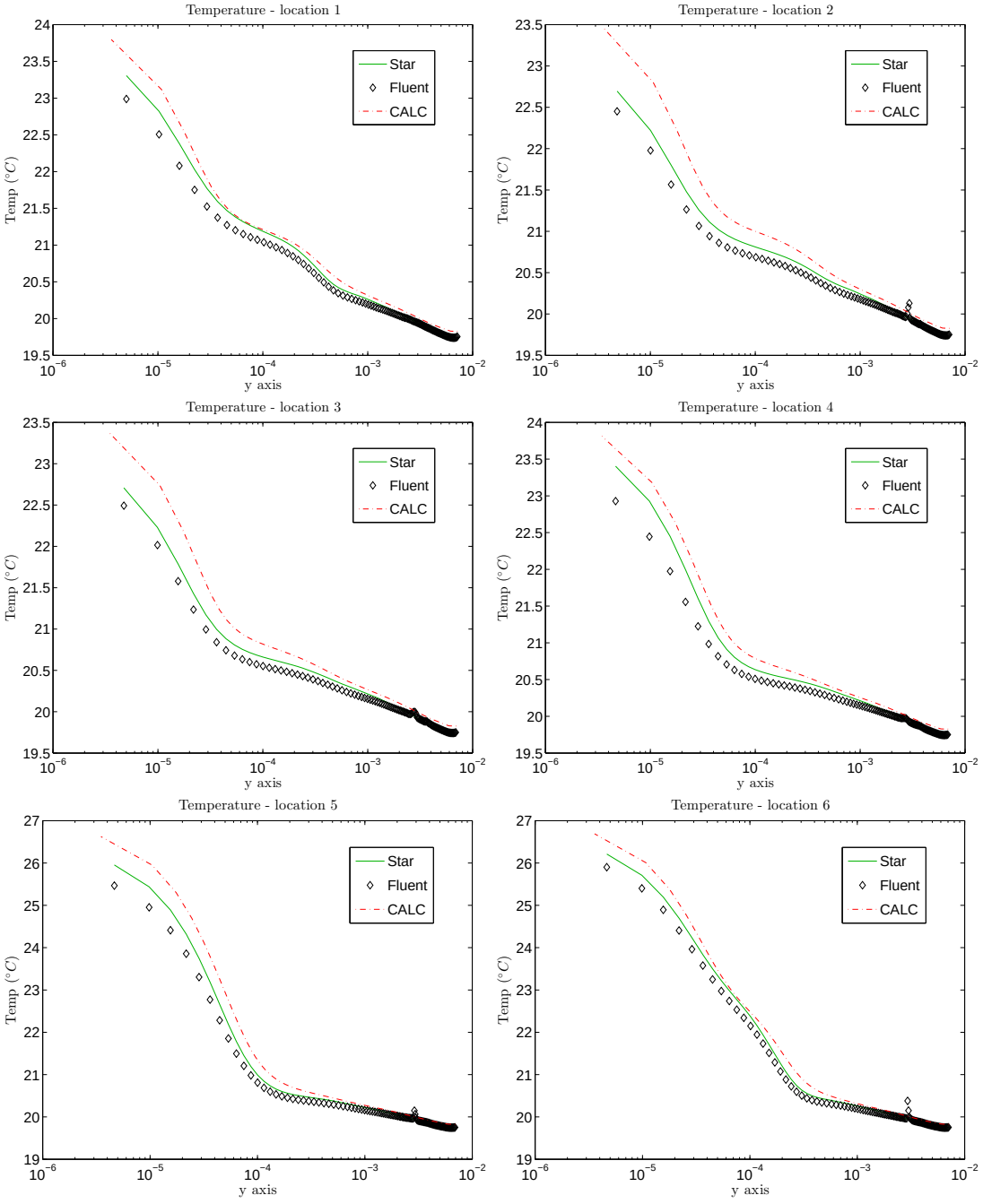

Figure 5.5: Logarithmic plots of the temperature $T\,(^{\circ}C)$ at six different locations for the all three solvers

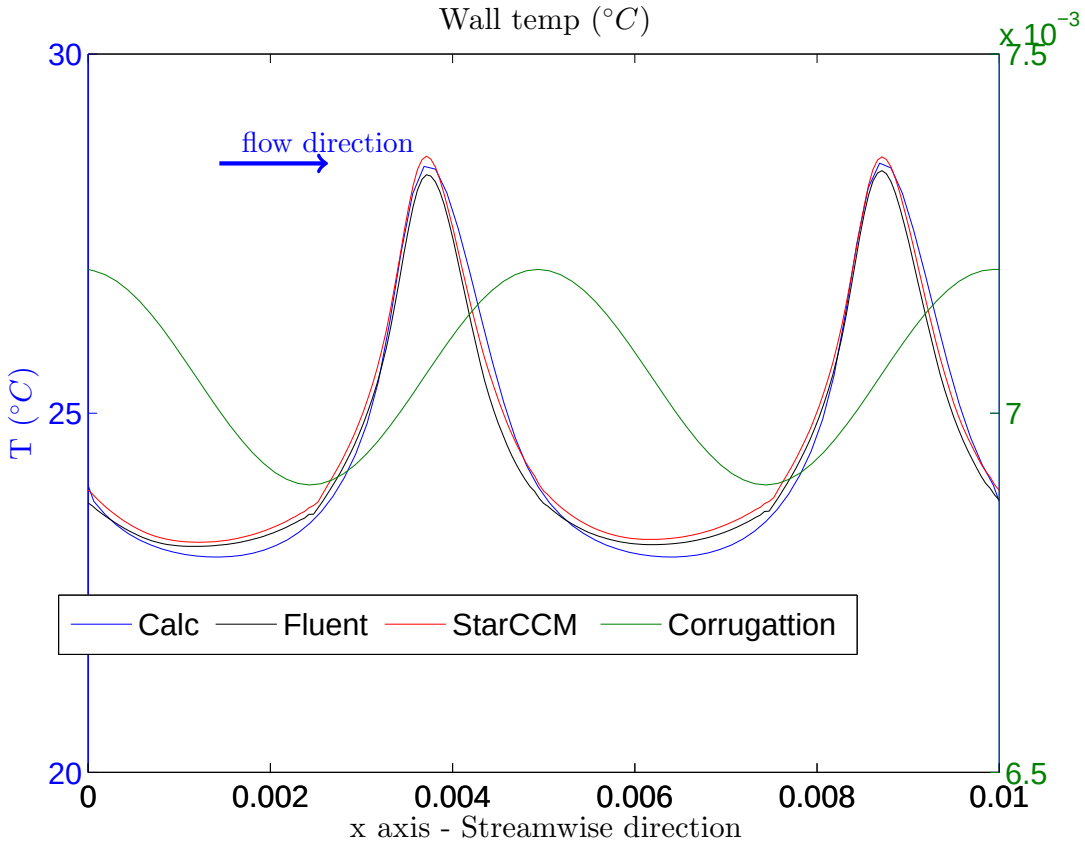

Figure 5.6: The wall temperature along the corrugation wall profile of the pipe.

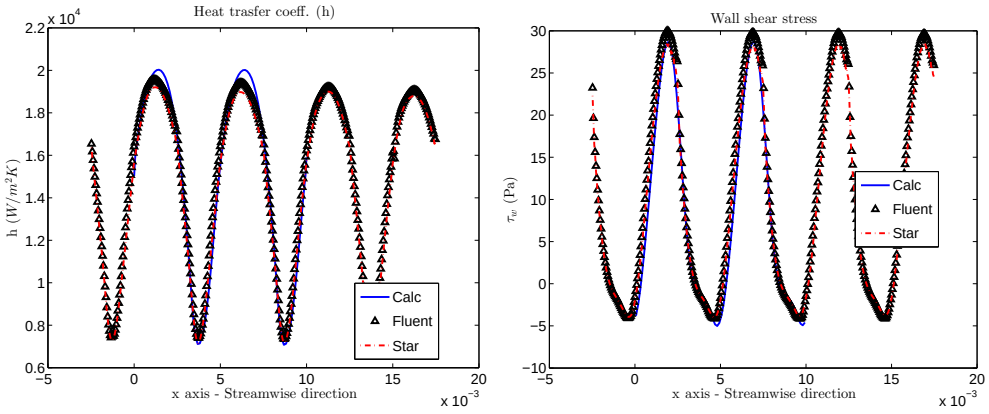

(a) Heat transfer coefficient, h

(b) Wall shear stress, τ_w

Figure 5.7: Variables along the stream wise direction(x axis) of the pipe

5.5 Conclusive remarks

A comparative values of the codes are given in table 5.2.

	CALC-BFC	Fluent	Star-CCM+
$\langle h \rangle$	14550	14800	14550
% difference	-	+1.72 %	+ 0%
$\langle \beta \rangle$	5200	5650	5350
% difference	-	+ 8.6 %	+ 2.9%

Table 5.2: Comparative values for validation of CALC code. Units : $\langle h \rangle - \mathrm{W/m^2K}$ and $\langle \beta \rangle - \mathrm{Pa/m}$

It is nice to realize that the values for the three different solvers are comparatively similar. Here it needs to be reminded that the CALC has a different mesh compared to ANSYS Fluent and STAR-CCM+, but the results are comparatively good. Moreover, the schemes used in the three solvers are different. Finally it was good to prove and validate the in-house solver, CALC-BFC, to further proceed with analysis of the pipe design. The in-house CALC solver has limitation of running on only one core, but its strength is its ability to be customized and versatile.

Chapter 6

Different cases of Numerical implementation

In this chapter different ways of implementing default case setting are presented. In section 6.1, the pressure source term in the momentum equation is implemented in two different ways and compared. In the latter section, a semi-circular pipe is simulated. These different case implementations were tried to investigate faster convergence with less simulation time.

6.1 Steady vs. unsteady pressure source term

A study was done to analyze the pressure source term that appears due to the streamwise periodic condition for any channel flow. In Patankar et al. [5], this source term β, equation 3.7 that occurs due to the pressure gradient in no-periodic flow is discussed in detailed.

The source can be kept as varying with time (unsteady) or kept as fixed value (steady). In the former case, the source term is varied to keep the mass flow fluctuations at the inlet of the pipe/channel constant. Thus, inlet bulk mass flow can be fixed rather than a result of simulation as in the case of Fröhlich et al. [19]. In the latter case, this fixed source term can be approximated from the drag as in Selvetti et al. [20]. However, in this thesis the fixed value is obtained from the converged source term, after running the simulations for some period of time.

The results presented for the CALC solver in this entire thesis, are with constant β while for Fluent and STAR they are with constant mass flow.

6.1.1 Inlet mass flow and pressure fluctuations

Figure 6.1(a) show the mass flow along the inlet of the pipe in case of unsteady pressure source, whereas, the corresponding mass flow for a fixed pressure source term is shown in the 6.1(b). The reader should not be misguided by the fluctuation from the required mass flow value in figure 6.1(b). It can be seen that the scale of the y axis in figure is small.

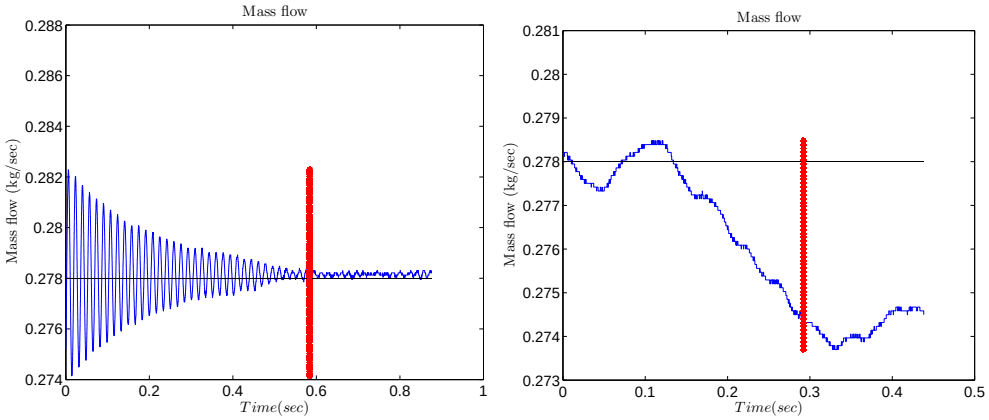

(a) Varying pressure source term case (b) Constant pressure source term case

Figure 6.1: Mass flow at the inlet of the pipe during the simulation time. The vertical red line gives the start of sampling.

6.1.2 Time-averaged terms along the streamline direction

Heat Transfer Coefficient. and Wall Shear Stress

The heat transfer and wall shear stress are compared for both the cases, as shown in figures 6.2(a) and 6.2(b). The wall shear stress seems to be exactly matching.

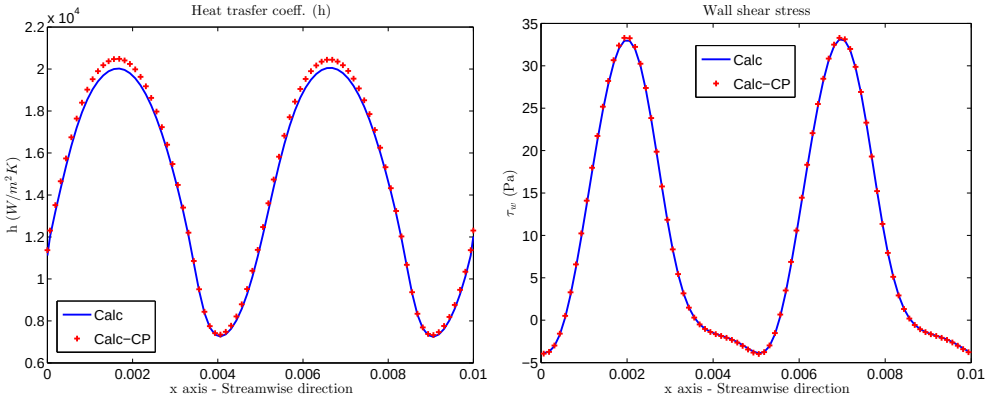

(a) Comparative Heat transfer coefficient (W/m^2K) (b) Comparative wall shear stress (Pa)

Figure 6.2: Here CALC - CP is the solver results with constant pressure condition

Nusselt number and Coefficient. of friction

The Nusselt number, Nu and the coefficient of friction are presented in figures 6.3(a) and 6.3(b).

Wall temperature

The wall temperature along the stream wise direction is also shown in figure 6.4.

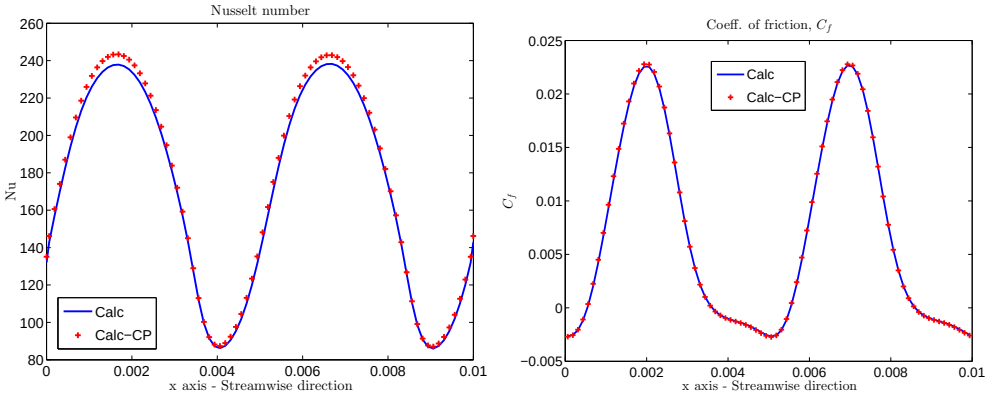

(a) Comparative Nusselt number, Nu_R (b) Comparative Coefficient of friction C_f

Figure 6.3: Here CALC - CP is the case with constant pressure condition

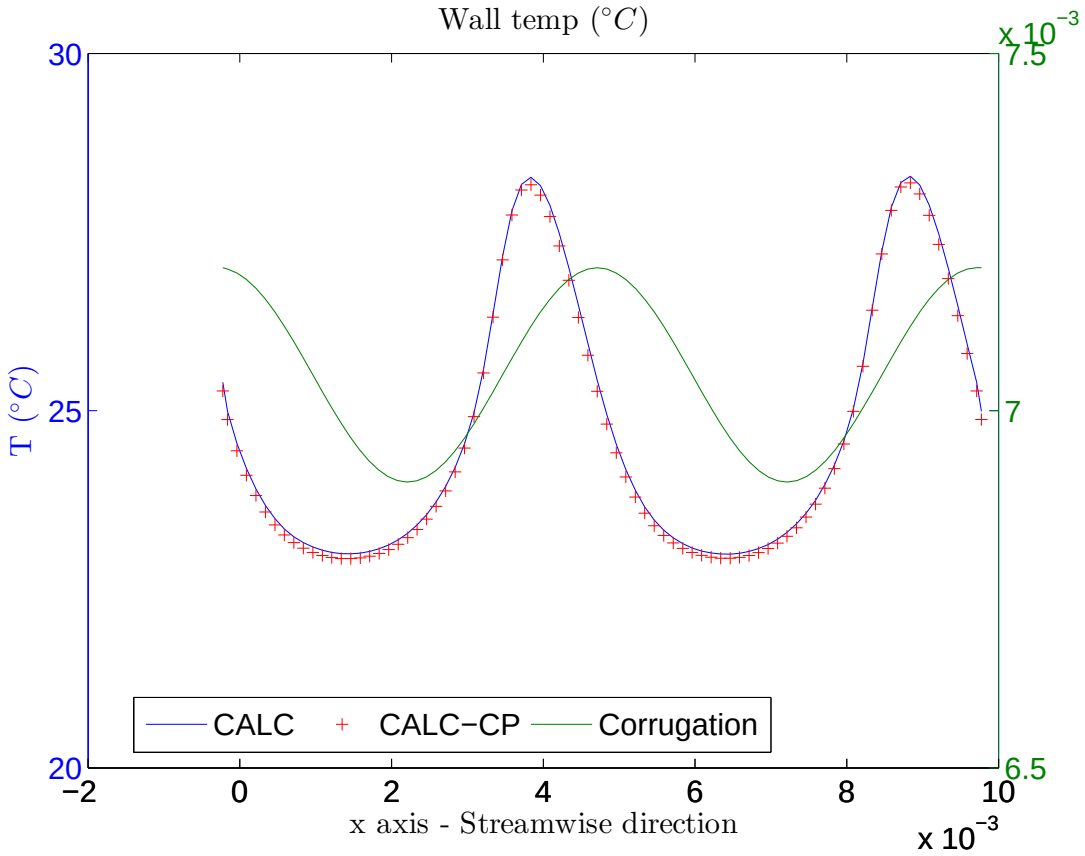

Figure 6.4: Comparative wall temperature ($°C$)along the corrugation profile of the pipe

6.1.3 Stresses and Pressure

The Reynolds normal stress, $\rho\overline{v_1'^2}$, shear stress, $\rho\overline{v_1'v_2'}$, and pressure terms are compared at six different locations as shown in Figures 6.5 (locations as in figure 5.1). It can be seen that variables are comparable.

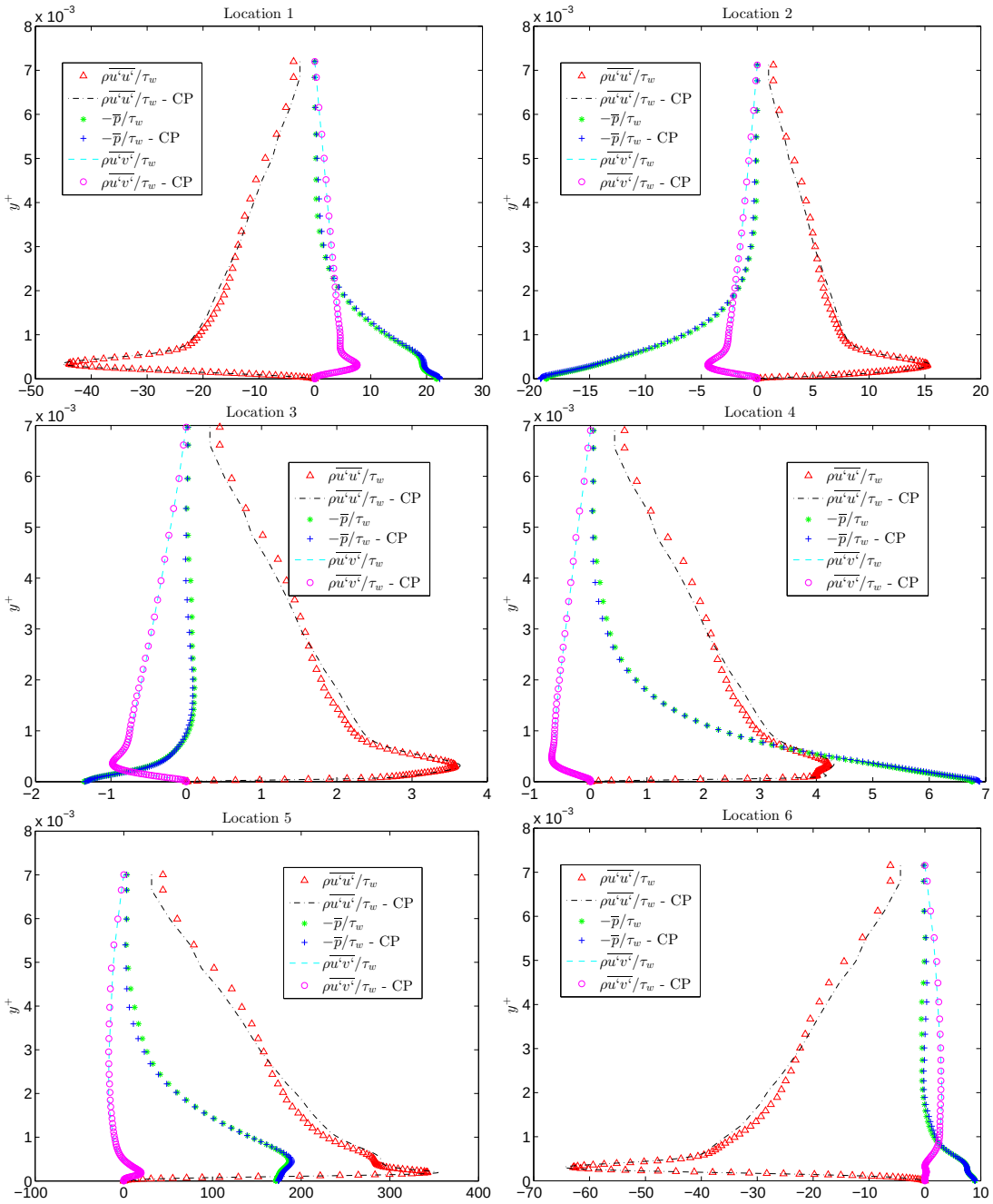

Figure 6.5: Reynolds stresses and pressure at six different locations

6.1.4 PDF of pressure

The pressure is monitored at an arbitrary chosen point in the flow domain, through out the simulation time to check the fluctuation of pressure variable for both cases.

Probability distribution function is chosen to illustrate the fluctuation of pressure at this point. The Gaussian distribution is given by,

$$f_{p'} = \frac{1}{p_{rms}} exp\left(-\frac{(p' - p_{rms})^2}{2p_{rms}^2}\right) \tag{6.1}$$

A probability density function with Gaussian distribution (L. Davidson [13, p. 61]), is shown in figure 6.6. As can be seen from figure, these distribution are matching really well.

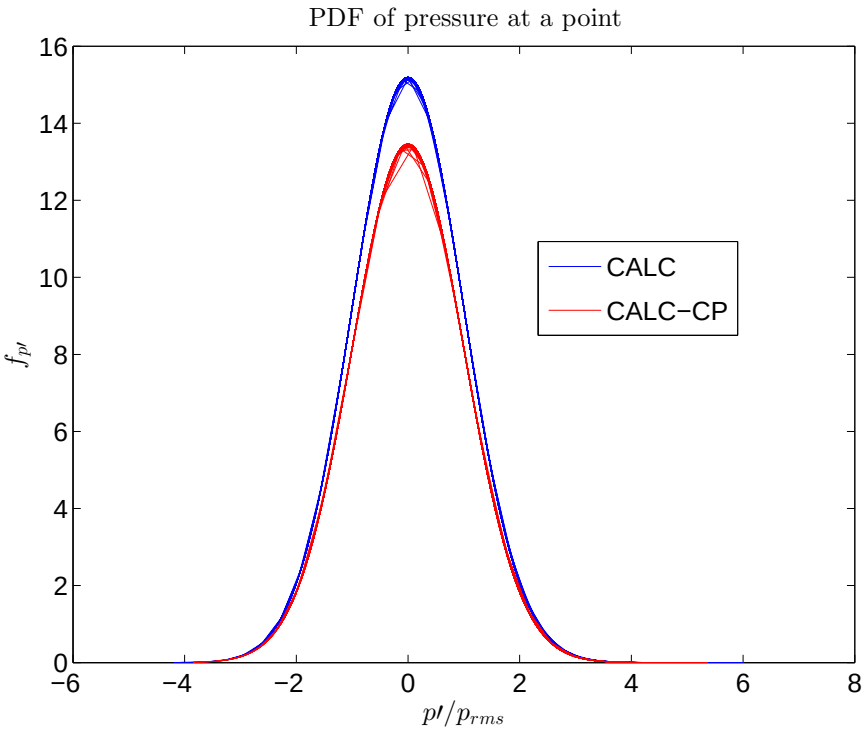

Figure 6.6: Probability density function of pressure at the point

6.1.5 Conclusive Remarks

This section has shown that both the implementations will give similar results. It can be suggested from the results gained that if the pressure source term is known prior to the simulation, it can implemented as constant source term in the momentum equation. This is supposed to dampen the fluctuations or instabilities that can occur during the simulation and thus attaining faster convergence. If the pressure source is allowed to vary with mass flow, the fluctuations in channel flow will take much longer time to die out.

6.2 Pumping effects in the half geometry

In order to reduce the computational time of the simulation, a semi-circular corrugated pipe was simulated with the CALC solver. In the thesis by Lindroth [21], it states after consideration of Nusselt number that a semi-circular pipe is a good aproximation

for full pipe. But, it was realized that pumping effects occurs when considering this geometry. The pumping effect can be shown by the inlet mass flow as in figure 6.7. It requires long time for this pumping to die, and thus loosing the purpose of attaining faster convergence through semi-circular symmetric geometry.

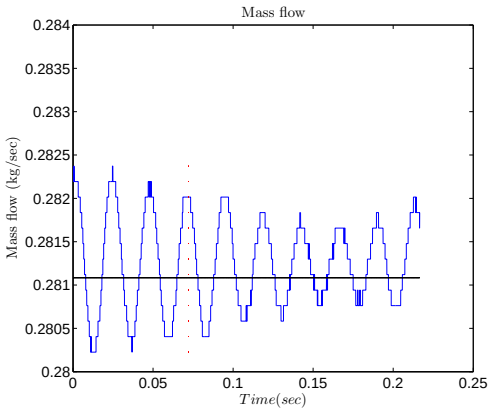

Figure 6.7: The pumping effect that occurs in the pipe when using a semi-circular geometry shown through inlet mass flow, kg/s

Chapter 7

Evaluating Mesh resolution

In large eddy simulation most of the eddies are resolved and some of them are modeled. Further refinement of the mesh will help in capturing the smaller eddies better, with the penalty of increased computational time. Also, as the mesh gets finer more eddies are resolved thus increasing the accuracy of the results. It is required to check whether the current results are mesh insensitive i.e, the results does not change when the mesh is finer. In order to evaluate the current default mesh for the CALC, mesh were made finer in y and z directions and were compared. The table 7.1 shows the data for the grid that are used.

Grid	Grid 1 - ref.	Grid 2	Grid 3
Node number (x,y,z)	$82 \times 82 \times 258$	$82 \times 98 \times 258$	$82 \times 82 \times 386$
x^+	8.52	8.36	8.53
y^+	0.24	0.20	0.24
z^+	12.04	11.83	8.04

Table 7.1: Grid 1 - the default case that was used in previous Chapter, Grid 2 - refined y direction and Grid 3 - refined in z direction(azimuthal).

Moreover, a DNS, i.e, simulations with no modeling is presented along with the refined meshes. This gives a deeper understanding of how far the eddies are resolved and modeled. The DNS is done on the Grid 3.

7.1 Near wall velocities

The near wall velocities for the default mesh to the refined meshes and DNS, are shown in figure 7.1. These figures are plotted along the wall normal directions at six different locations as shown in figure 5.1.

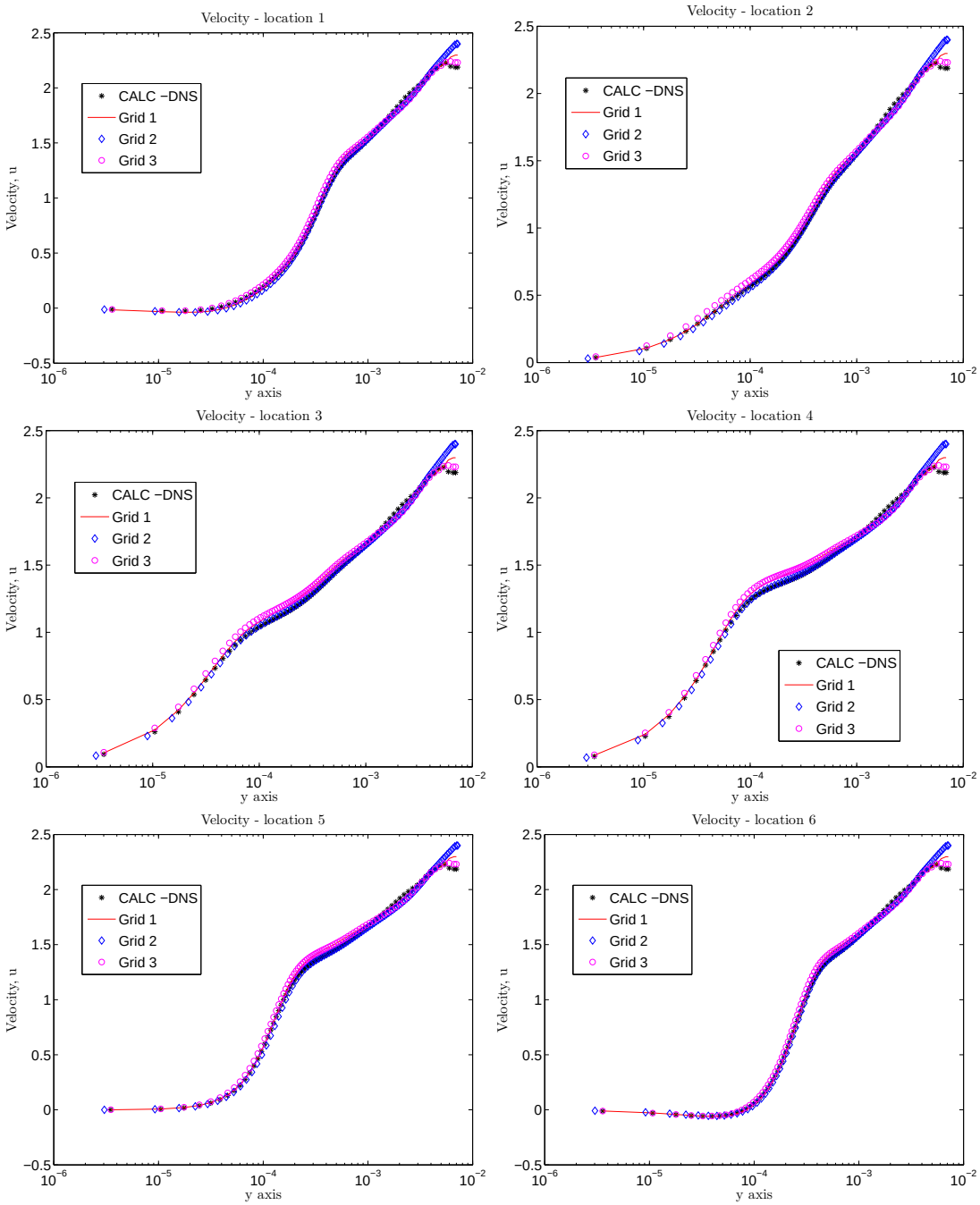

Figure 7.1: Near wall logarithmic plots of the stream wise velocity $u\,\mathrm{or}(v_1)\,\mathrm{m}^2/\mathrm{s}$.

It can be observed that, near the wall, the velocity profiles for the refined meshes match well with the default mesh. Near the center of the flow some of the velocities are over-predicted or under-predicted in few nodes. It may die out if the simulation ran for some time. But, under time constrain for the current thesis it was not investigated further. The most importance inference to be gained was the validation of the current default mesh. The DNS also matches well with the default mesh which goes on to suggest that most of the eddies are resolved.

7.2 Resultant variable along the Wall profile

7.2.1 Wall temperature

In order to validate the sensitivity of thermal distribution to mesh variation, wall temperatures were compared. These wall temperatures along the corrugation profile of the pipe are shown in figure 7.2.

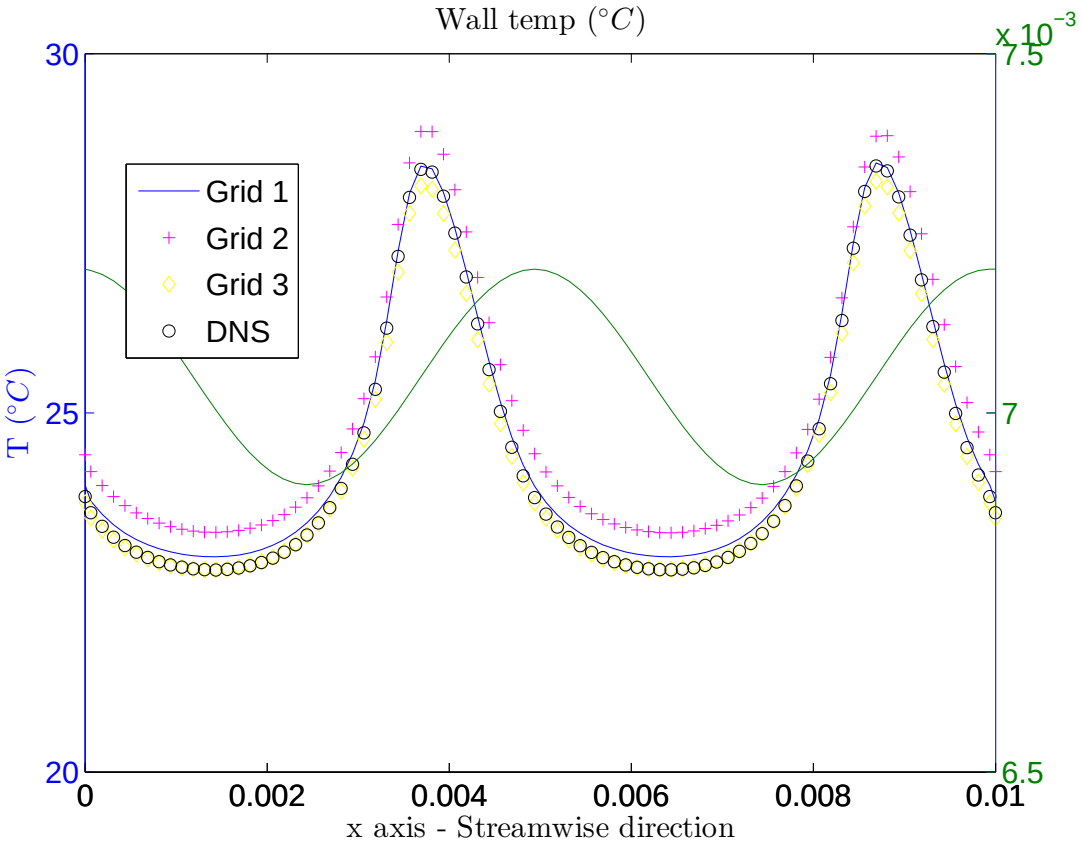

Figure 7.2: The wall temperature along the corrugation wall profile of the pipe.

The wall temperature for the refined meshes shows a slight mis-match at some locations, but nothing drastic that needed attention. Thus, it stands as a good argument for the stating that current default mesh is good.

7.3 Heat Transfer coefficient and Wall shear stress

Here we further compare the more sensitive variables which supports the validation of the current mesh. Heat transfer is computed from the wall temperature and bulk temperature. Thus, given the fact that heat flux is constant, bulk temperature also comes into picture and play a important role when comparing the heat transfer coefficient.

Also, since the wall shear stress is computed from the velocities at the walls and adjacent cell, it is quite sensitive to mesh near the walls. Thus, heat transfer coefficient and wall shear stress along the flow direction are shown in figures 7.3(a) and 7.3(b) respectively.

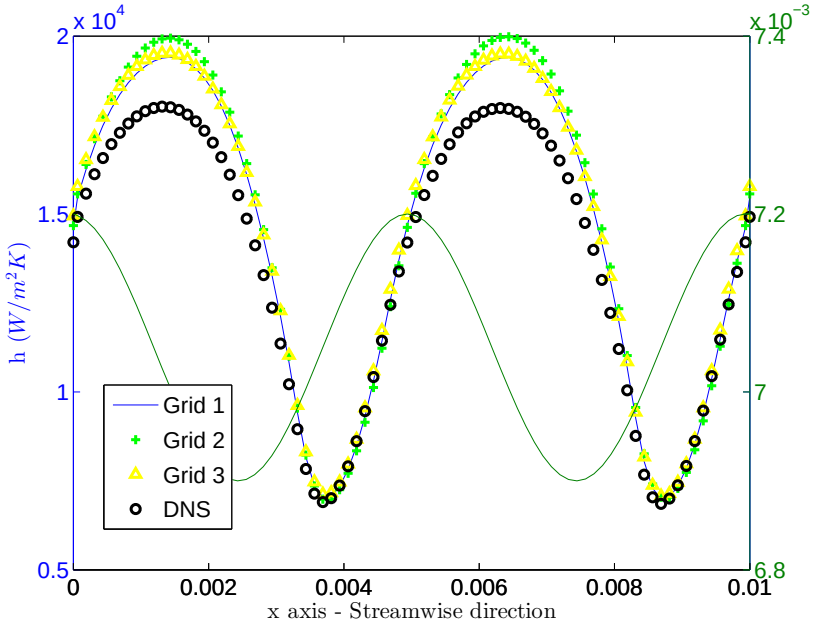

(a) Heat transfer coefficient, h

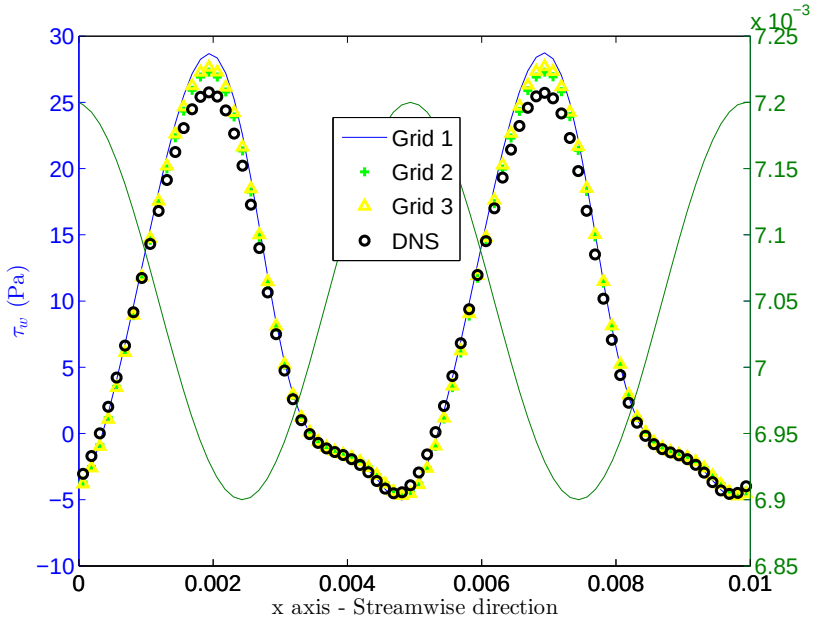

(b) Wall shear stress, τ_w

Figure 7.3: Along the corrugation wall profile of the pipe

As previously mentioned, since both the variable are really sensitive to the accuracy of the solution and as these variable are matching really well, it becomes more clear that the default mesh is really good. However, the heat transfer coefficient for the DNS have not converged enough to match well with the default mesh.

7.4 Nusselt number and Coefficient of friction

Nusselt number and coefficient of friction are non-dimensional counterparts of the above mentioned heat transfer coefficient and wall shear stress. It has been illustrated in figures 7.4(a) and 7.4(b).

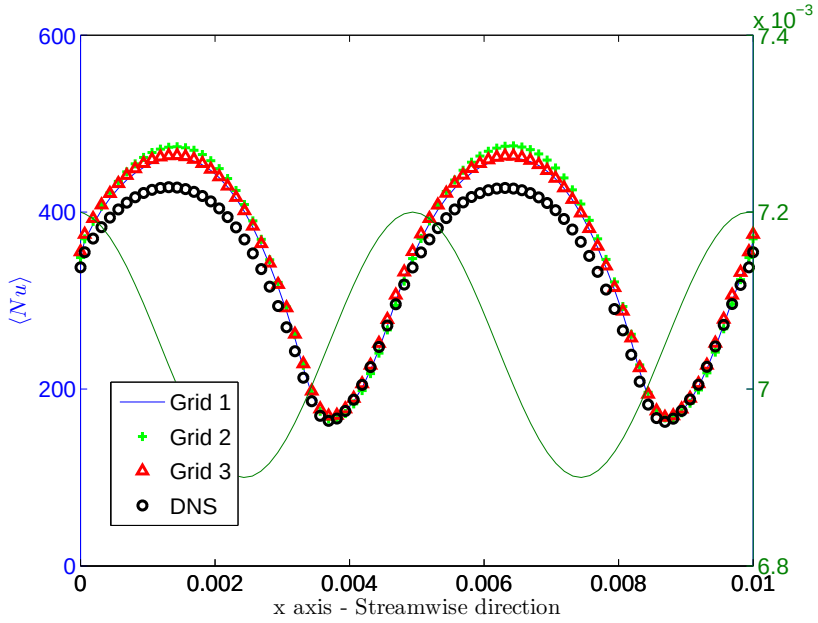

(a) Nusselt, $\langle Nu \rangle$

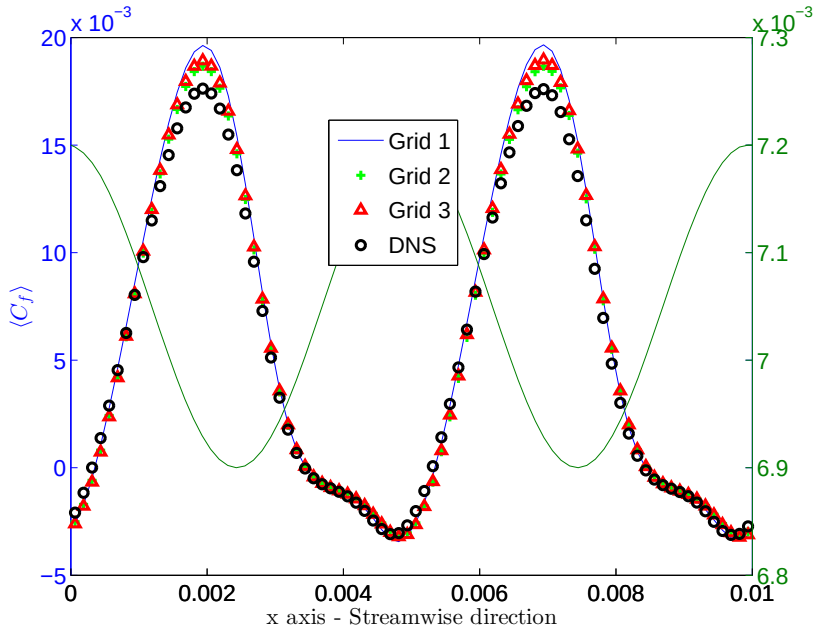

(b) Coefficient of friction, C_f

Figure 7.4: Along the corrugation wall profile of the pipe

7.5 Conclusive remarks

In the case of large eddy simulation it was often discussed and analyzed to what extend the eddies are captured. As the mesh goes finer it is able to capture the smaller eddies. But the current refinement did not give any drastic change to the global parameters that was important for the study as can be seen from table 7.2. Thus the current mesh was proceeded for the flow and thermal analysis for the corrugated pipes.

Grid	Grid 1 - ref.	Grid 2	Grid 3
Node number (x,y,z)	$82 \times 82 \times 258$	$82 \times 98 \times 258$	$82 \times 82 \times 386$
$\langle Nu \rangle$	368	350	362
$\langle C_f \rangle$	5.977e-3	5.671e-3	5.739e-3
$\langle h \rangle$	14500	14750	14700

Table 7.2: Grid 2- refined y direction and Grid 3- refined in z direction(azimuthal).

Chapter 8

Flow and Thermal analysis

8.1 Flow and turbulence

Once the in-house CALC-BFC solver and mesh were well validated in the previous chapters, this chapter digs into analysing the flow physics with turbulent and heat transfer enhancement by the corrugations of a pipe. Flow in the corrugated pipe is studied through large eddy simulation with stream-wise periodic boundary condition. Along the wavy walls of the pipe, turbulence is studied in the separation, re-circulation and reattachment regions. This chapter involves varies generalized study from Fröhlich et al. [19] and Choi et al. [22]. It needs to be noted that all variables are in non-dimensional form as per CALC-BFC. These dimensionless variables were discussed previously in the section 4.

8.2 Flow analysis

Corrugations to the pipe enhances the turbulence in the pipe. The influence of this turbulence can be budgeted through stress calculation at the different location of the pipe. The Reynolds stresses at six different location, as in figure 5.1, are given in figure 8.1 and their surface plots are shown in figures 8.2 and 8.3. The quantitative value of the stress can be seen in figure 8.1 and their distribution is illustrated by surface plots in figures 8.2 and 8.3.

At entry of the pipe, i.e at location 1, it can be seen from figure 8.1(a) that the streamwise stress is much larger than the others. But as the we move along the corrugation from location 1 to location 4, this normal stress reduces. This reduced stress in the streamwise direction is distributed to the wall normal and shear stresses through the pressure strain term [13].

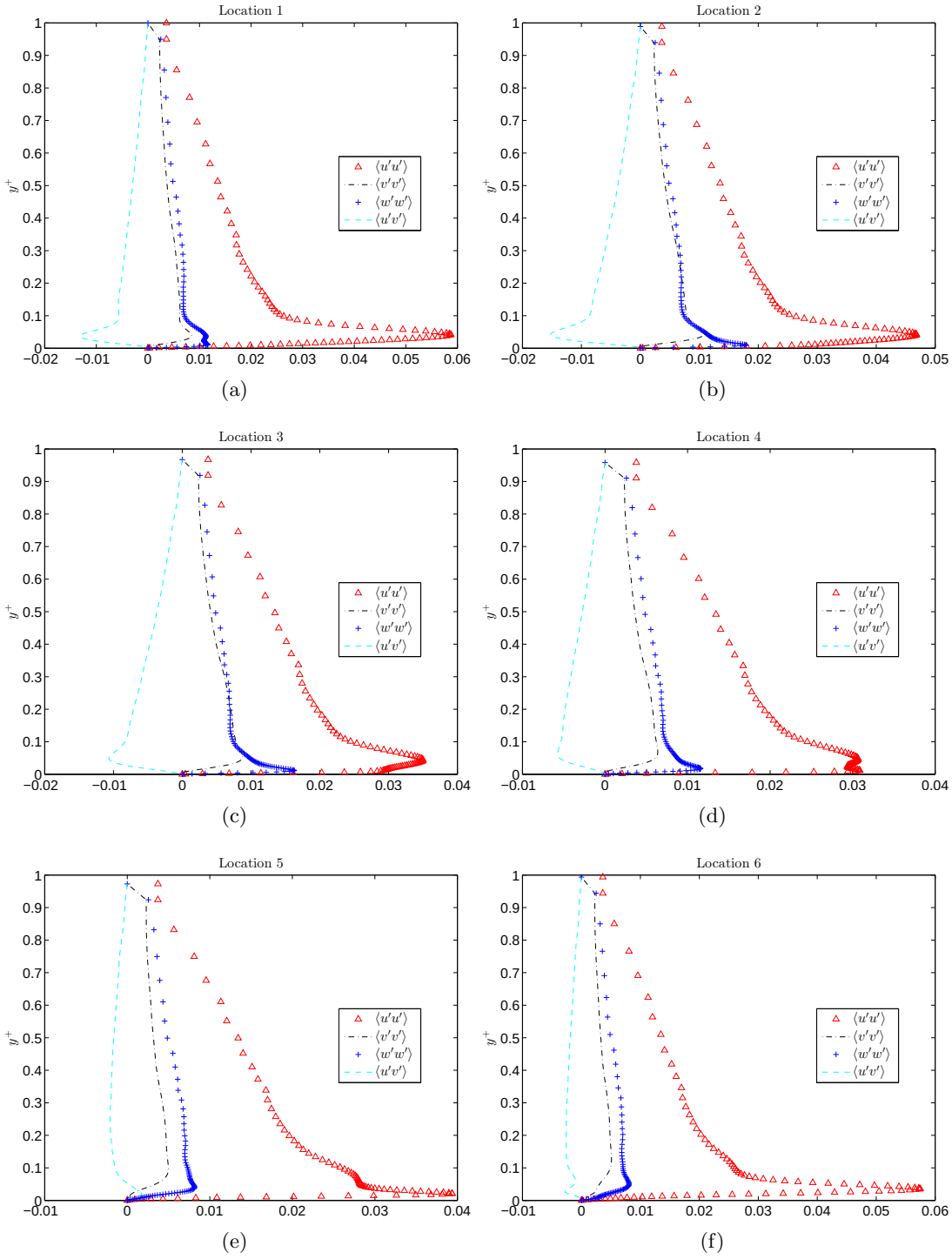

Figure 8.1: Reynolds stresses at six different locations

Figures 8.3(a) and 8.3(b) shows that the spanwise stress, $\langle w'w' \rangle$, increases at the downhill sections of the wave wall. Here the downhill of the corrugation can also be termed as the flow impinging section, since it forces the flow in the streamwise direction to teh wall normal direction. Thus, when the flow encounters the impinging wall, streamwise gushing flow is deviated in the wall normal and spanwise direction.

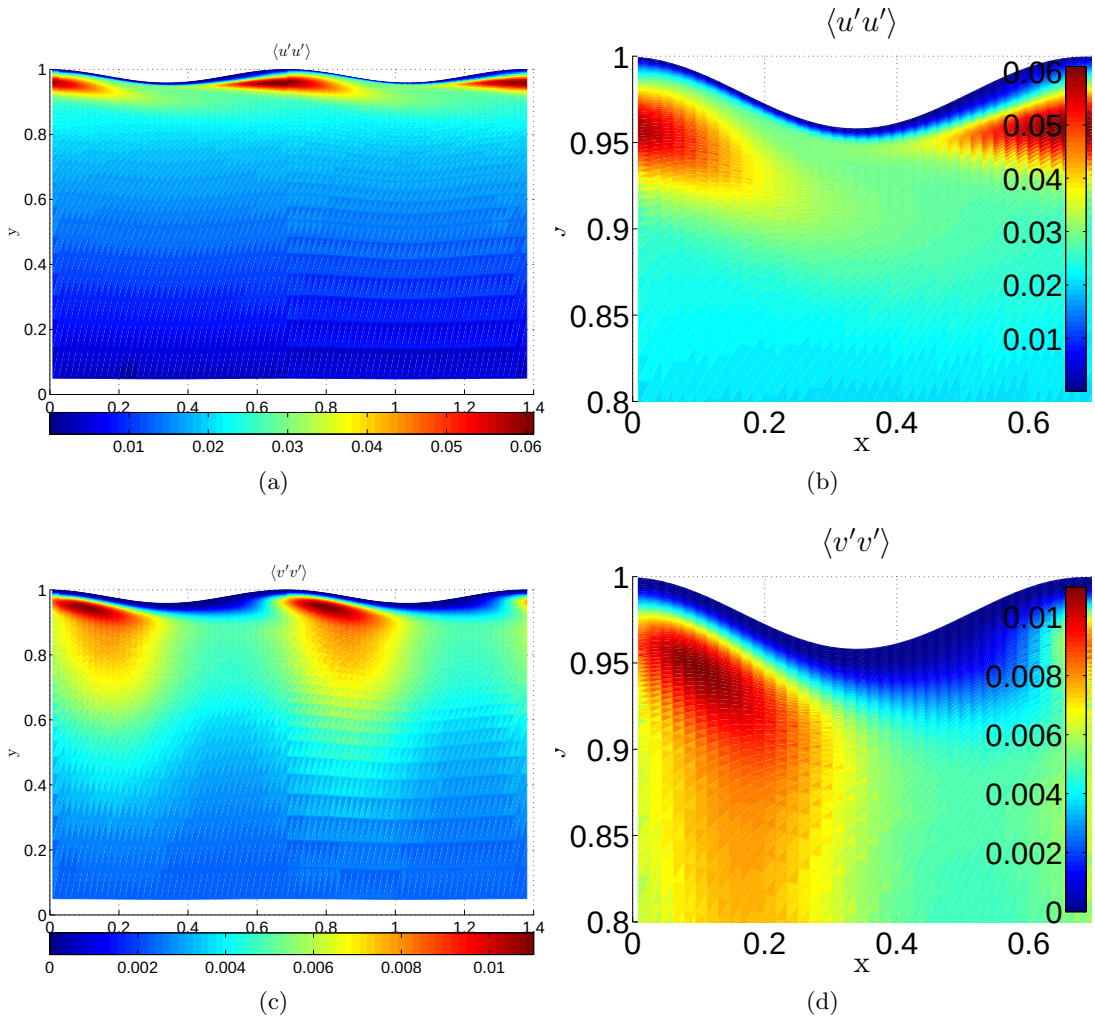

Figure 8.2: Stresses along the domain, time and azimuthally averaged

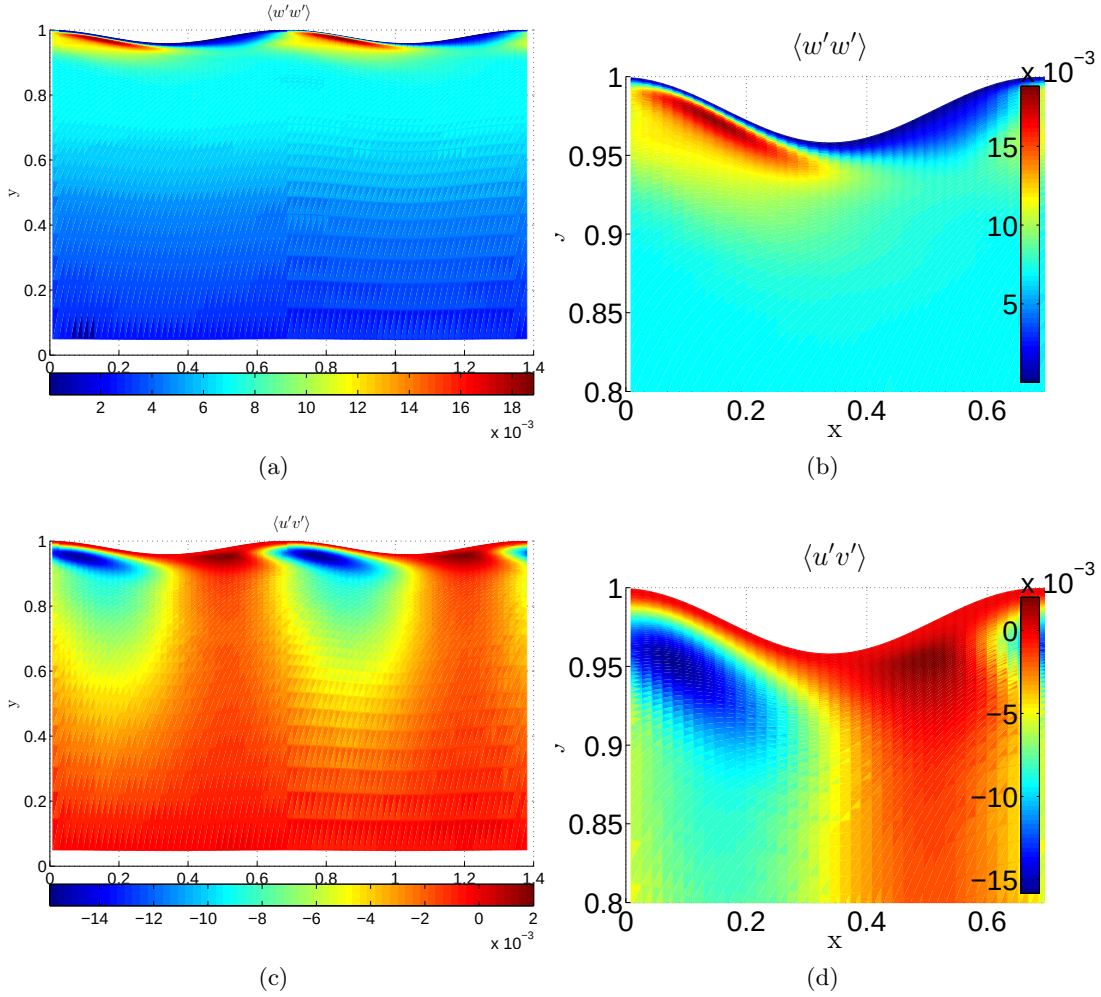

Figure 8.3: Stresses along the domain, time and azimuthally averaged

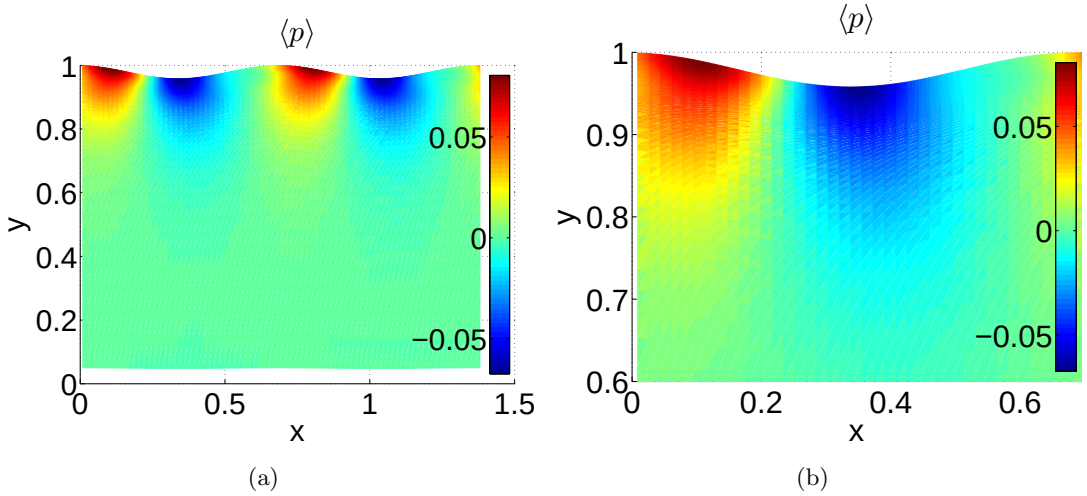

Figure 8.4: Pressure along the domain, time and azimuthally averaged

This phenomenon has been illustrated through the stress distribution from $\langle u'u' \rangle$ to $\langle v'v' \rangle$ and $\langle w'w' \rangle$. Thus, streamwise and spanwise eddies are both formed.

Spanwise eddies have been shown in figure 5.4(a). Formation of eddies can be explained in quite different ways. One good explanation is differential distribution of localized pressure along the walls of the wavy pipe as can be seen in figures 8.4. The negative localized pressure at the downhill on the corrugation sucks the flow from the main stream flow, this pulls the flow into the uphill section of the wavy wall. Here concave curve of the corrugation curls the flow to form eddies. Also, when the flow hits the walls at the downhill section of the pipe, it is distributed in the wall normal direction, spanwise direction and upwind directions. This phenomenon is same as a water jet hits a wall. When the water jet hits the wall, it is splashed in the all directions. Similar flow phenomenon is experienced in the downhill section of the corrugation.

Spanwise eddies are also created in areas of high spanwise stress. These eddies are shown through vector plots of v and w in figure 8.5. The vectors gives a clear picture of the re-circulation in both clockwise and counter-clockwise direction. It can also be seen that regions between two adjacent eddies will have either wall normal or radial flow. Also, the circulations gets stronger as flow approaches the downhill region of the corrugated profile. However, these eddies are really small compared to their spanwise counterparts. The streamwise eddies cancel each other when averaged in the spanwise direction, but it can turn out to be interesting when corrugations are helical.

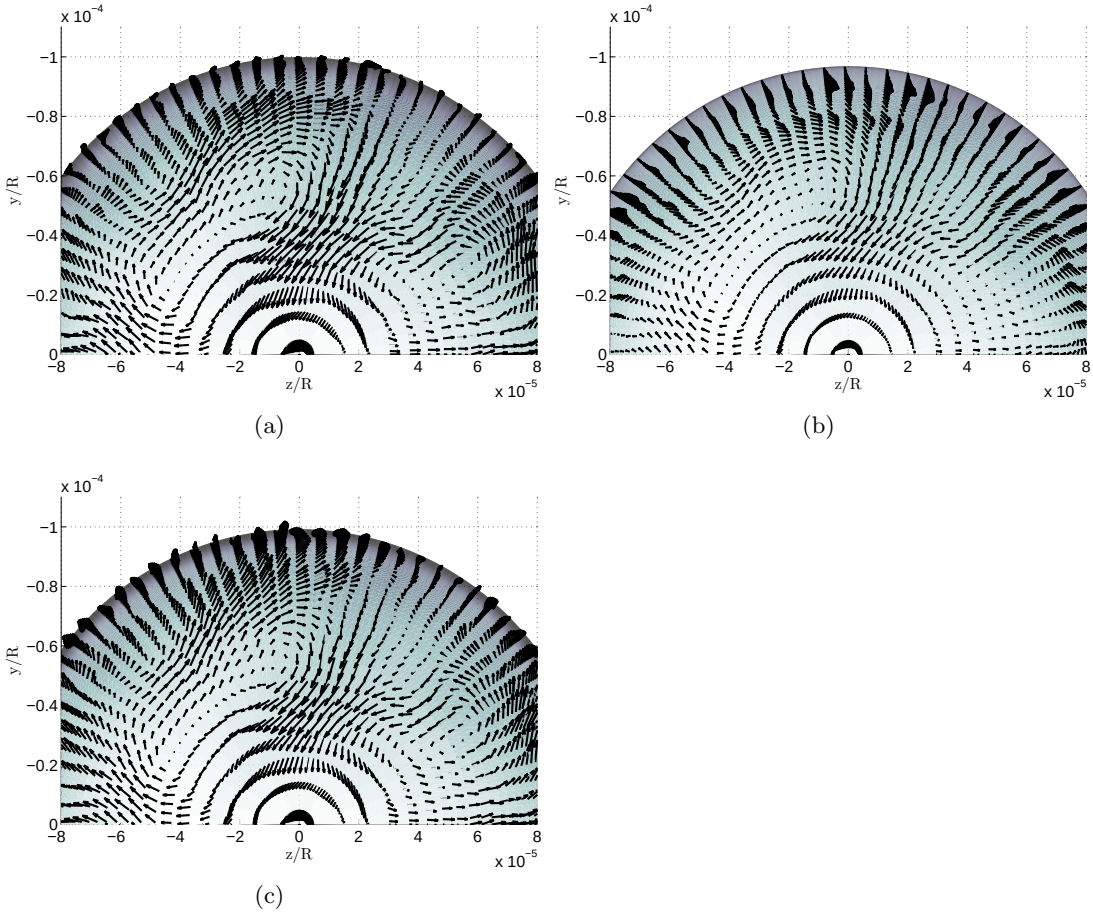

Figure 8.5: Streamwise circulations with wall normal and spanwise velocities as vectors at three different streamwise locations. The figure is shaded by streamwise velocity, u, with the darker shade for the lower values.

8.3 Thermal analysis

Distribution of the heat fluxes in the domain is analysed in this section. Viscous and turbulent fluxes are shown in figure 8.6 and SGS and convective fluxes are shown in figure 8.7. The viscous fluxes are only dominant near the walls of the corrugation. Due to the corrugation of the pipe there exist spanwise eddies with recirculating convective fluxes. This in-turn enhances the heat transfer coefficient of the pipe.

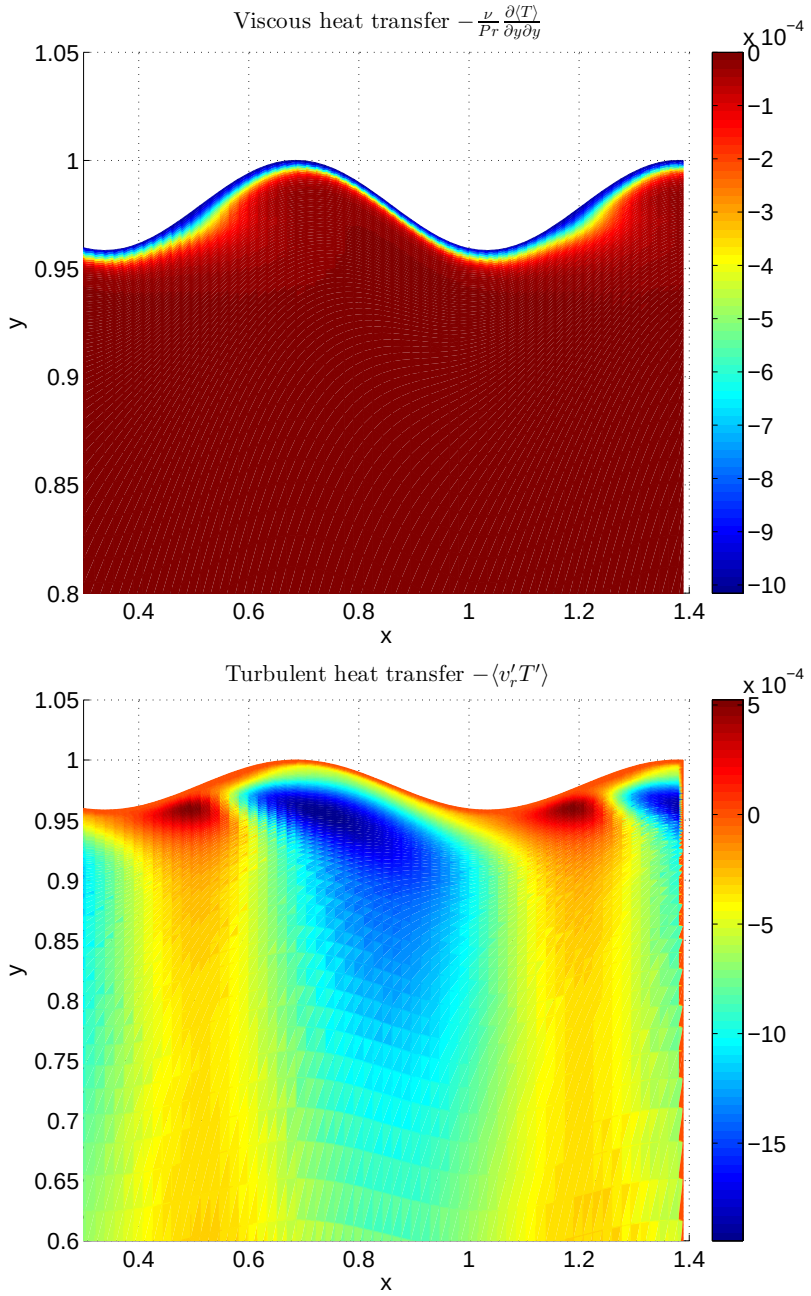

Figure 8.6: Viscous and turbulent fluxes

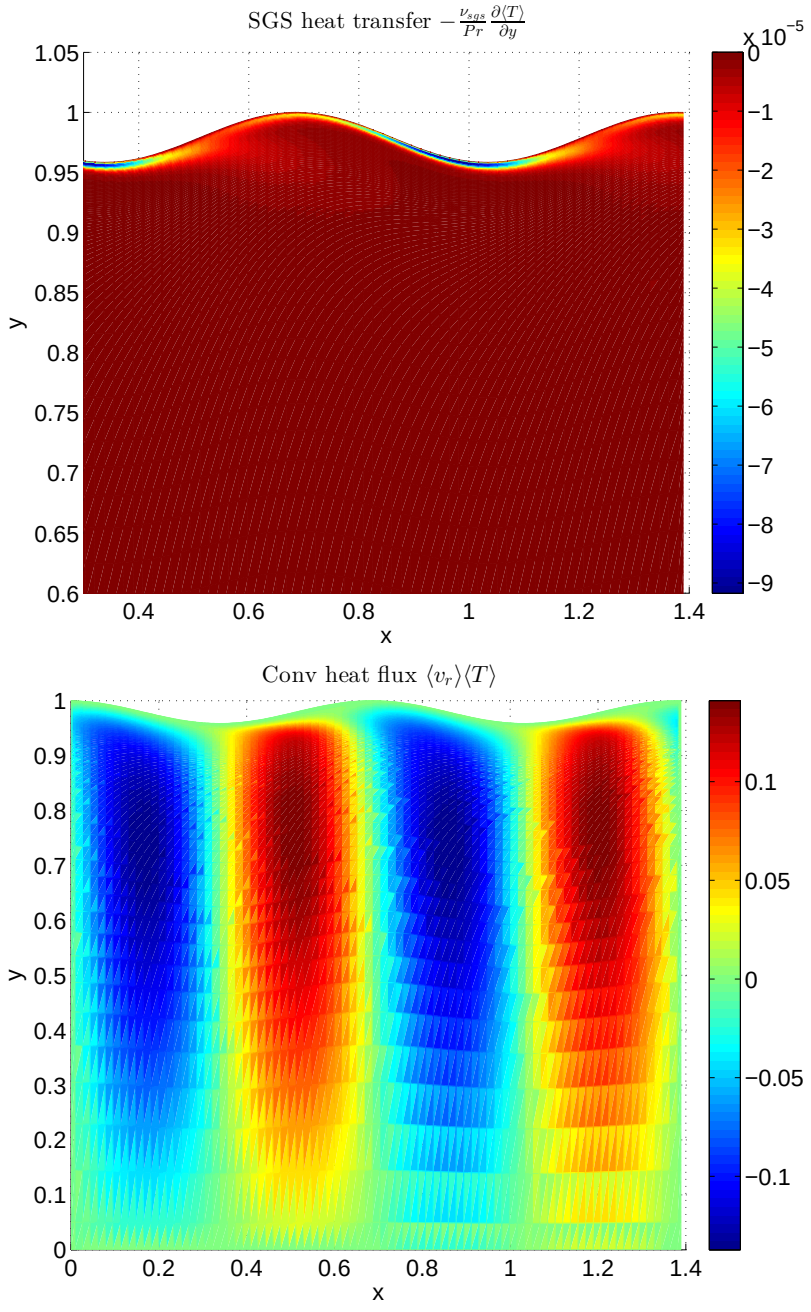

Figure 8.7: SGS and convective fluxes

Chapter 9

Geometrical changes to the corrugation

Once physical and thermal characteristics of flow was understood it was interesting to know the effect of corrugation height ($2a$) to turbulent and thermal enhancement. The table 9.1 shows four additionally different corrugation profiles that were studied. Out of four, two of them have their corrugation height reduced from the default; i.e, protrusion to the flow is reduced. In the latter two, corrugation height is increased and thus supposed to increase the disturbance to flow. The corrugation heights are changed while keeping the outer radius constant and varying inner radius.

Cases	2a	ϕ
Reference	0.3	6.250e-04
Case 1	0.2	2.778e-04
Case 2	0.25	4.340e-04
Case 3	0.35	8.507e-04
Case 4	0.4	11.111e-04

Table 9.1: Different corrugation height (2a) and ϕ is the severity index (Section 1.1)

9.1 Variables along the wall profile

As similar to the studies conducted along this whole thesis work, the variables are studied along the corrugation profile.

9.1.1 Heat Transfer coefficient and Wall shear stress

The heat transfer coefficient and the wall shear stress along the length of the pipe, are shown in figures 9.1(a) and 9.1(b) respectively. It can noticed that HTC increases with increasing corrugation height with the penalty of increased wall shear stress. It was also interesting to notice the little shift in the peak of the HTC with change in corrugation height.

9.1.2 Nusselt number and Coefficient of friction

The non-dimensional variables Nusselt number and coefficient of friction are shown in figure 9.2(a) and 9.2(b).

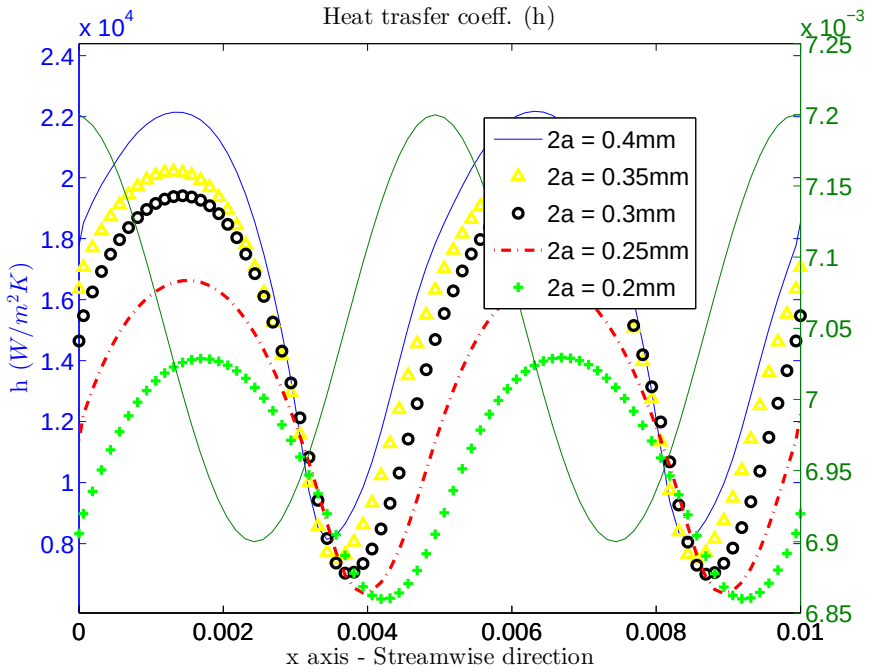

(a) Heat transfer coefficient, h

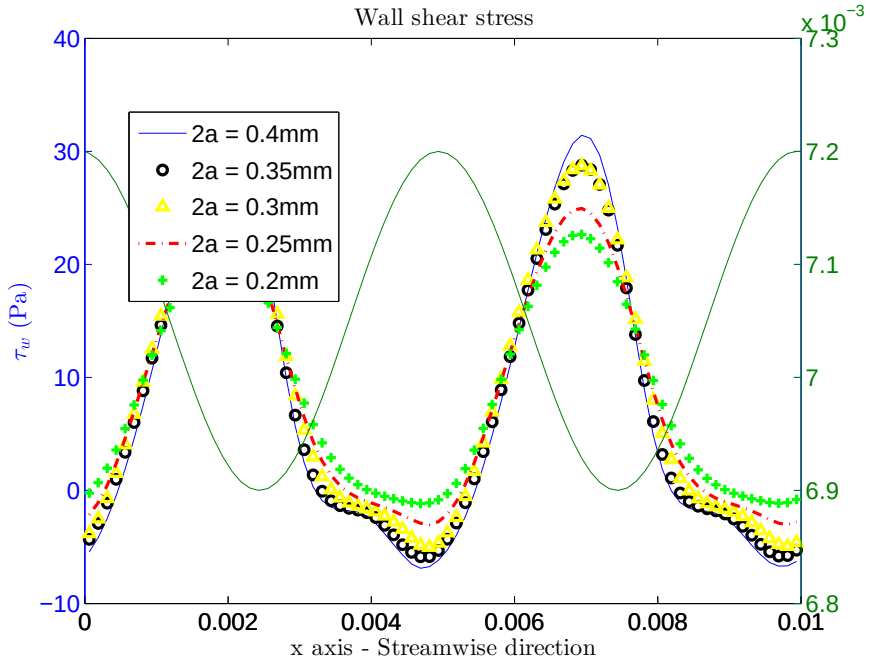

(b) Wall shear stress, τ_w

Figure 9.1: Heat transfer coefficient and the wall shear stress along the corrugated wall profile of the pipe. The green solid line is the default corrugation profile.

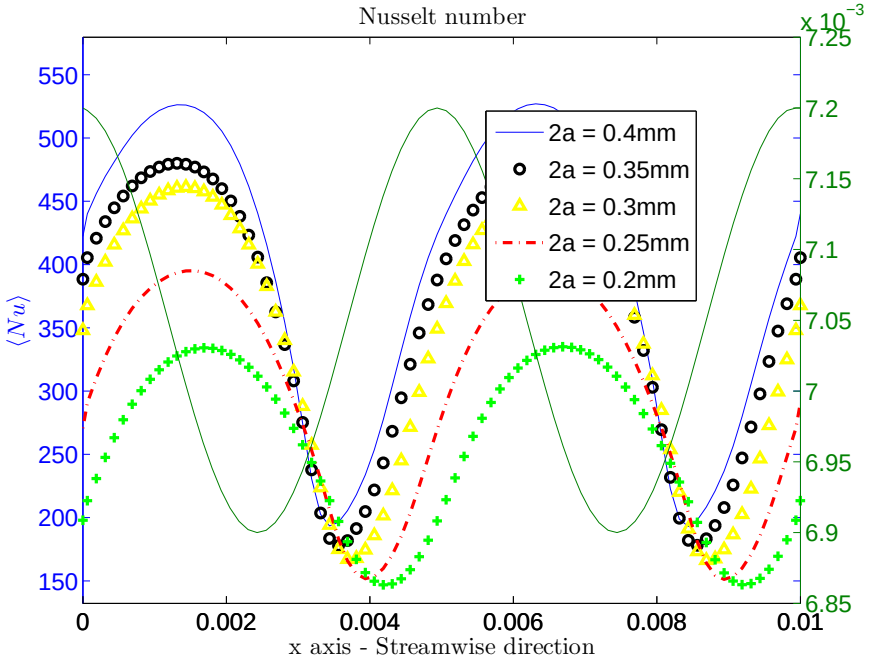

(a) Nusselt, $\langle Nu \rangle$

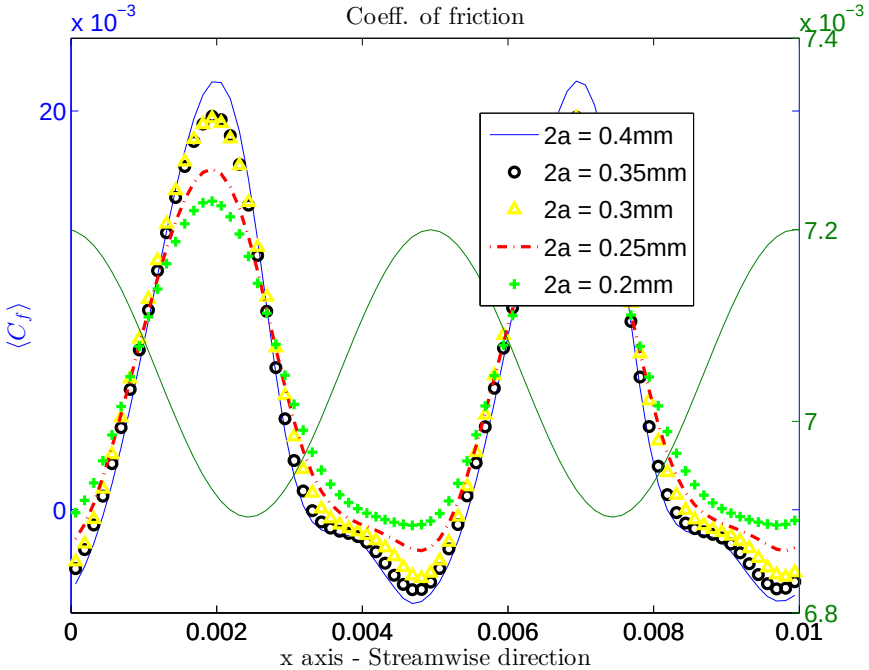

(b) Coefficient of friction, C_f

Figure 9.2: Nusselt number and coefficient of friction along the corrugation wall profile of the pipe. The green solid line is the default corrugation profile.

9.2 Conclusive summary

It can be concluded that the heat transfer and turbulence is enhance by increasing the corrugated height while keeping constant outer radius. With increment of the heat transfer which is good for a heat exchanger, there exist a penalty of increased differential pressure for the flow, as seen from values in table 9.2. The heat transfer coefficient and pressure from table is well illustrated in figures 9.3(a) and 9.3(b). This goes on to suggest that, it requires a pump with greater power that can attain additional pressure to have the enhanced heat transfer.

While talking on efficiency of a heat exchangers, it is general practice to discuss on the basis of an universal criteria. These are termed as Performance Evaluation Criteria (PEC). This criteria serves as single independent optimization variable to compare the efficiency of different designs of heat exchangers. Several performance evaluation criteria were proposed by Bergles *et al.* [23] [24], and Webb *et al.* [25]. These parameters are derived based on dimensionless parameters that have been taken into consideration, the enhancement of heat transfer and compromise given on friction and pressure. One such performance criteria is JF, which is used for comparison here. This criteria is given for different goemetries in table 9.2s.

Cases	Reference	Case 1	Case 2	Case 3	Case 4
$\langle Nu \rangle$	340	250	300	360	400
$\langle C_f \rangle$	5.73e-3	5.98e-3	5.80e-3	5.47e-3	5.39e-3
$\langle h \rangle$	14550	10600	12400	15350	16700
$\langle \beta \rangle$	5200	3500	4100	5900	7100
$\langle j \rangle$	0.0069	0.005	0.0059	0.0073	0.0079
$\langle JF \rangle$	2.31	1.69	1.98	2.44	2.66

Table 9.2: Units : $\langle h \rangle$ – W/m^{2}K, $\langle \beta \rangle$ – Pa/m, $\langle j \rangle$ - Colburn Number, $\langle JF \rangle$ - Performance index

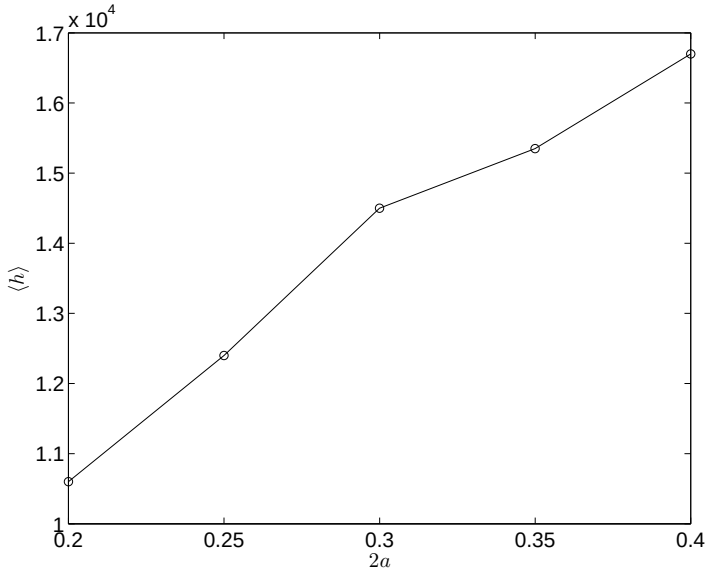

(a) Heat transfer coefficient, h

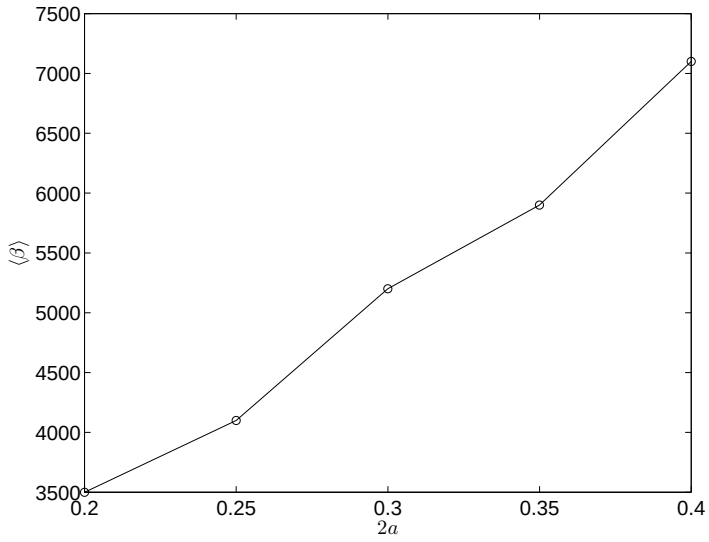

(b) Pressure source, $\langle\beta\rangle$

Figure 9.3: Rate of change of HTC and pressure source with corrugation height ($2a$).

Chapter 10

Conclusions

Numerical results of turbulent effects and heat transfer enhancement of three dimensional periodic wavy pipe is presented in the current thesis. A Reynolds number, $Re_b = 13610$ and constant heat flux are given to the pipe. Using large eddy simulation the in-house CALC-BFC solver is compared with the commercial ANSYS Fluent and STAR-CCM+. The modelling was also validated with varying mesh and DNS. The whole thesis work can be summarised as:

1. It was important to analyse the solver variations and understand the effect of different numerical implementation of the solvers. Comparison for codes in the Section 5 gives a good explanation of the same.

2. Whenever modeling the fluid flow using LES, it is interesting to know, how far the eddies are resolved. Thus in the chapter 7 refined meshes are simulated and compared to give good estimation of the resolved eddies.

3. It was also interesting to analyse the fluid and thermal flow in the pipes. It is explained through the stress distribution in the domain. It was also interesting to know the effect of corrugation in the flow domain.

4. In the last chapter 9, the corrugation height is varied keeping the outer radius constant. It was realised that increasing the height of the corrugation will disturb the flow, increasing turbulence and heat transfer. But, at the same time there is increase of pressure source that comes as penalty. It will be interesting to analyse the trade-off point at which it comes as a optimum. Performance criteria gives a good idea about which corrugation profile is optimum.

Bibliography

[1] P. Vicente, A. Garcia, and A. Viedma, "Experimental investigation on heat transfer and frictional characteristics of spirally corrugated tubes in turbulent flow at different prandtl numbers," *International Journal of Heat and Mass Transfer*, vol. 47, no. 4, pp. 671 – 681, 2004.

[2] M. Mirzaei, L. Davidson, A. Sohankar, and F. Innings, "The effect of corrugation on heat transfer and pressure drop in channel flow with different prandtl numbers," *International Journal of Heat and Mass Transfer*, vol. 66, no. 0, pp. 164 – 176, 2013.

[3] M. Mirzaei, A. Sohankar, L. Davidson, and F. Innings, "Large eddy simulation of the flow and heat transfer in a half-corrugated channel with various wave amplitudes," *International Journal of Heat and Mass Transfer*, vol. 76, no. 0, pp. 432 – 446, 2014.

[4] R. Shah and A. London, "Thermal boundary conditions and some solutions for laminar duct flow forced convection," *Journal of Heat Transfer*, vol. 96, no. 2, pp. 159–165, 1974.

[5] S. V. Patankar, C. H. Liu, and E. M. Sparrow, "Fully developed flow and heat transfer in ducts having streamwise-periodic variations of cross-sectional area.," *ASME J. of Heat Transfer*, vol. 99, no. 2, pp. 180–186, 1977.

[6] Tetrapak, "Tetra spiraflo ®c: Model cm." http://www.tetrapak.com/usprocessing/heat-exchangers/tubular-heat-exchangers/tetra-spiraflo-cm-heat-exchanger.

[7] Tetrapak, "Tetra spiraflo ®c: Model cm."

[8] D. Tritton, *Physical Fluid Dynamics*. Oxford Science Publications, Clarendon Press, 1988.

[9] L. Reichl, *A Modern Course in Statistical Physics*. Wiley, 2009.

[10] J. Reddy, *An Introduction to Continuum Mechanics*. Cambridge University Press, 2007.

[11] P. Emvin, *The full multigrid method applied to turbulent flow in ventilated enclosures using structured and unstructured grids*. PhD thesis, Dept. of Thermo and Fluid Dynamics, Chalmers University of Technology, Göteborg, 1997.

[12] L. Davidson and S.-H. Peng, "Hybrid les-rans modelling: a one-equation sgs model combined with ak–ω model for predicting recirculating flows," *International Journal for Numerical Methods in Fluids*, vol. 43, no. 9, pp. 1003–1018, 2003.

[13] L. Davidson, "Turbulene modelling.," 2013.

[14] M. Germano, U. Piomelli, P. Moin, and W. Cabot, "A dynamic subgrid-scale eddy viscosity model.," *Phys. Fluids*, vol. A, no. 3, pp. 1760–1765, 1991.

[15] D. K. Lilly, "A proposed modification of the germano subgrid-scale closure method.," *Phys. Fluids*, vol. A, no. 4, pp. 633–635, 1992.

[16] A. Wray and J. Hunt, "Algorithms for classification of turbulent structures.," *Topological Fluid Mechanics: Proceedings of the IUTAM Symposium.*, pp. 95–104, 1989.

[17] F. Ducros, F. Nicoud, and T. Poinsot, "Wall-adapting local eddy-viscosity models for simulations in complex geometries," in *Proceedings of 6th ICFD Conference on Numerical Methods for Fluid Dynamics*, pp. 293–299, 1998.

[18] F. Nicoud and F. Ducros, "Subgrid-scale stress modelling based on the square of the velocity gradient tensor," *Flow, Turbulence and Combustion*, vol. 62, no. 3, pp. 183–200, 1999.

[19] J. Fröhlich, C. P. Mellen, W. Rodi, L. Temmerman, and M. A. Leschziner, "Highly resolved large-eddy simulation of separated flow in a channel with streamwise periodic constrictions," *Journal of Fluid Mechanics*, vol. 526, pp. 19–66, 2005.

[20] M. Salvetti, R. Damiani, and F. Beux, "Three-dimensional coarse large-eddy simulations of the flow above two-dimensional sinusoidal waves," *International journal for numerical methods in fluids*, vol. 35, no. 6, pp. 617–642, 2001.

[21] D. Lindroth, "Large eddy simulation of flow and heat transfer in a pipe with corrugated walls.," 2013.

[22] H. S. Choi and K. Suzuki, "Large eddy simulation of turbulent flow and heat transfer in a channel with one wavy wall," *International journal of heat and fluid flow*, vol. 26, no. 5, pp. 681–694, 2005.

[23] A. Bergles, A. Blumenkrantz, and J. Taborek, "Performance evaluation criteria for enhanced heat transfer surfaces.," *Jpn Soc of Mech Eng,Tokyo*, pp. 234–238, 1974.

[24] A. Bergles, R. Bunn, and G. Junkhan, "Extended performance evaluation criteria for enhanced heat transfer surfaces," *Letters in Heat and Mass Transfer*, vol. 1, no. 2, pp. 113 – 120, 1974.

[25] R. Webb, "Performance evaluation criteria for use of enhanced heat transfer surfaces in heat exchanger design," *International Journal of Heat and Mass Transfer*, vol. 24, no. 4, pp. 715 – 726, 1981.